Precision Measurement of the η Mass

WEIGHTED AVERAGE
547.54±0.13

GEM/COSY (2005)
NA48/CERN (2002)
TAPS/MAMI (1995)
SPES4/SATURNE (1992)
Rutherford Lab. (1974)

η mass (MeV/c^2)

Annual Report 2005

Institut für Kernphysik / COSY

Cover picture:
Ideogram of the η-mass based on the compilation of the Particle Data Group and the recently published value of the GEM collaboration. The disagreement of the NA48 result with all other data triggered the precision measurement of the GEM collaboration making use of the high brilliance COSY beam matched with the high resolution magnetic spectrograph BIG KARL. The present GEM result defines the width of the lower mass branch while the upper one is given by the NA48 result.

Preface

The year 2005 has been a challenging one for the institute: as a consequence of the "mixed results" of the first review in February 2004 within the Research Programme "Physics of Hadrons and Nuclei" in the Research Field "Structure of Matter" of the Helmholtz Centres, IKP was faced with substantial cuts in resources for 2005. An even more serious threat ensued with possible further reductions for the years 2006 – 2009, depending, however, on the outcome of an "in-depth" evaluation of the IKP activities.

The review on "COSY and FZJ contributions to FAIR", conducted by an international committee, and headed by Peter Paul (BNL, USA), took place on two days in April 2005. IKP presented its strategy for the further use of COSY and, in close collaboration with GSI (Darmstadt), the cooperation towards the construction of the FAIR facility. In its report, issued later last year, the committee almost fully supported our plans, and as a result and the financial agreements, which have been negotiated in the meantime, we now have a solid basis for the remainder of the first funding period (2006 – 2009). — I would like to take this opportunity to thank all who contributed to this great success in one way or the other.

One of the explicit recommendations of the committee was to give green light for the relocation of the WASA detector from CELSIUS (Uppsala, Sweden) to COSY. The detector dismount at TSL and transfer to FZJ was completed in 2005, and we are now in the process of installing WASA at an internal target station of COSY — more details are given in the main text. Commissioning of WASA is scheduled to begin in the second half of 2006 and first experiments are expected to start in 2007.

In connection with the WASA-at-COSY project, the IKP had decided to reduce the amount of COSY beamtime for users in 2005 by about 2000 hours. The increased downtime is needed to install WASA in the COSY ring, but also has the positive side-effect that the cost-savings will be used to finance necessary maintenance and upgrades of WASA detector components and electronics. This was part of the financing concept which has been worked out between the IKP directorate and the FZJ board of management.

On the scientific frontier, IKP has made a number of important contributions (details can again be found in the main text):

- The ANKE collaboration has found indications for a heavy hyperon state $Y^{0*}(1480)$ in the analysis of $pp \to pK^+\pi X$ at a beam momentum of 3.65 GeV/c.

- The GEM collaboration has determined the mass of the η meson with unprecedented accuracy, exploiting the reaction $pd \to {}^3\text{He}\eta$ and simultaneously $pd \to t\pi^+$ at the BIG KARL magnetic spectrometer (see cover picture and corresponding article).

- At COSY the efficiency for flipping the proton spin by means of a small rf dipole has been pushed to more than 99.9%.

- The intensity of the polarized ion source for H^- was raised to $50\,\mu\text{A}$, thus doubling its original specification.

The involvement of the IKP in the FAIR project to be realized at the GSI was fully honored by the committee. Our efforts are focused on the design and construction of the High Energy Storage Ring (HESR) and significant contributions to the PANDA-detector. We are dedicated to make this endeavor a success being aware of its great potential to advance hadron physics and connected fields during the next decades.

We have been able to meet the challenges of 2005 not only due to our own efforts, but because we could rely on the support and advice of many people. I like to express our gratitude to all of them, the colleagues from the infrastructure of our Research Center (FZJ) in particular ZAM, ZAT, and ZEL, the people from the universities and research centers from Germany and all over the world and, last but not least, the CANU community.

Jülich, February 2006   Hans Ströher

Contents

Appendix

1 Physics at COSY

1.1 Overview

Currently, COSY harbors four experiments at internal target stations — **ANKE**, **COSY-11**, **EDDA** and **PISA** — as well as two external facilities — **BIG KARL** (with ENSTAR, GEM and HIRES) and **COSY-TOF**.

ANKE and **COSY-11** are magnetic spectrometers with a wide momentum acceptance for charged particles. They are both well suited to study meson-production processes close to thresholds with particle emission into forward direction. At the non-magnetic **EDDA** detector $\vec{p}\vec{p}$ elastic scattering has been studied and the device is now being used as a beam polarimeter. **PISA** has been used for the investigation of spallation processes induced by GeV protons. **BIG KARL** is a high resolution magnetic spectrometer which is supplemented by the GEM and ENSTAR detectors at larger emission angles. The non-magnetic spectrometer **COSY-TOF** measures the velocity and direction of charged particles with large angular acceptance thus allowing for the kinematically complete reconstruction of events with up to one neutral particle. So far all detectors at COSY are "photon-blind". This will change with the **WASA** detector which is planned to be commissioned at COSY in fall 2006. **WASA** can detect both neutral and charged particles with a large angular and momentum acceptance. **WASA**, **ANKE** and **COSY-TOF** will be the only detector systems at COSY after 2006.
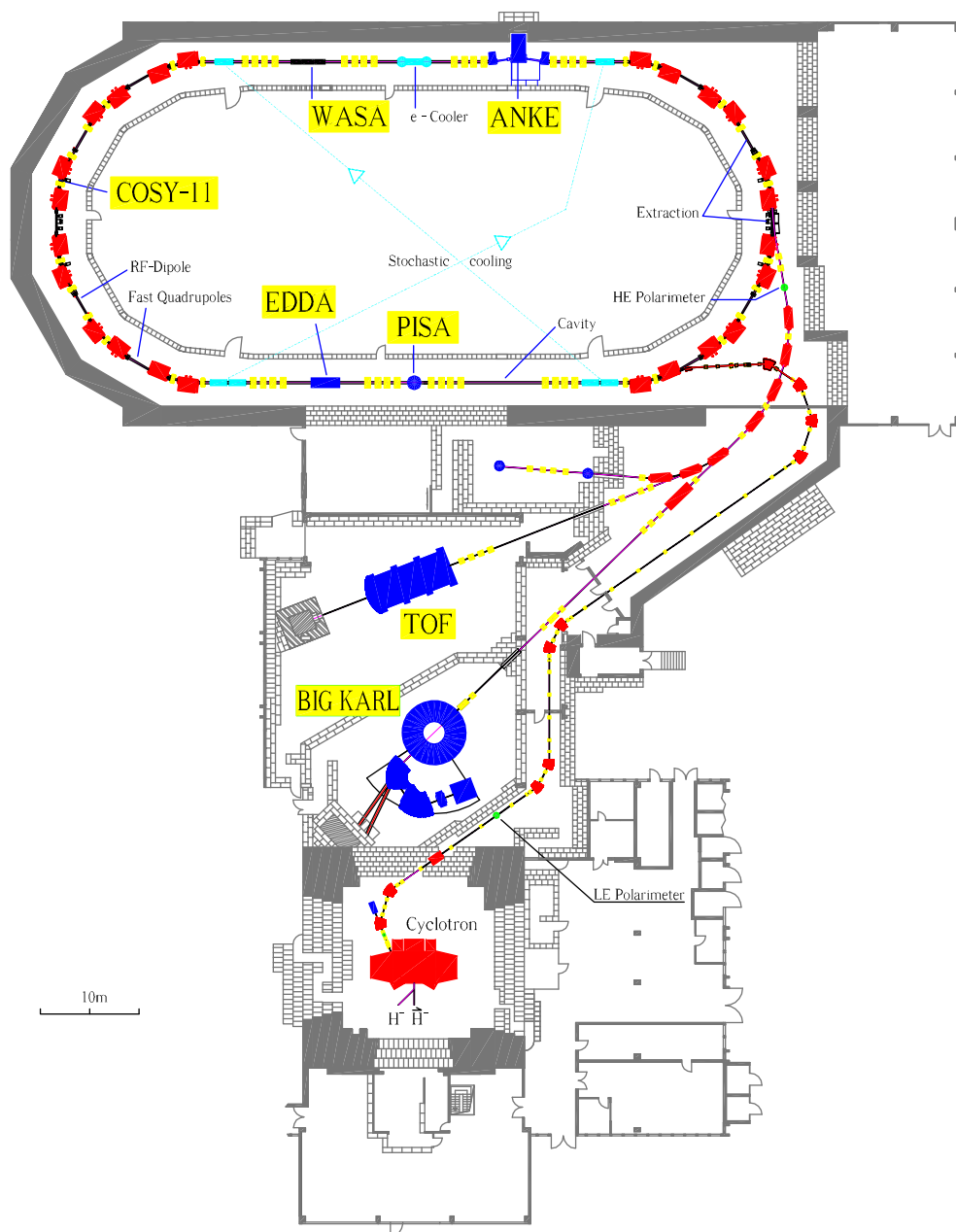
1.2 Major Physics Results at COSY

1.2.1 Precision measurement of the η-mass

Compared to other light mesons, the mass of the η is surprisingly poorly known. Though in 2004 the Particle Data Group (PDG) quotes a value of $m_\eta = 547.75 \pm 0.12$ MeV/c^2, this error hides differences of up to 0.7 MeV/c^2 between the results of some of the modern counter experiments. The PDG average is in fact dominated by the result of the CERN NA48 experiment, $m_\eta = 547.843 \pm 0.051$ MeV/c^2, which is based upon the study of the kinematics of the six photons from the $3\pi^0$ decay of 110 GeV η-mesons. In the other experiments employing electronic detectors, which typically suggest a mass ~ 0.5 MeV/c^2 lighter, the η was produced much closer to threshold and its mass primarily determined through a missing-mass technique where, unlike the NA48 experiment, precise knowledge of the beam momentum plays an essential role. In the experiment at Rutherford Laboratory, the momentum of the pion beam in the $\pi^- + p \to n + \eta$ reaction was fixed macroscopically using the floating wire technique. In the photoproduction reaction $\gamma + p \to p + \eta$, the energy of the electrons that were the source of the bremsstrahlung photons was fixed to a relative precision of 2×10^{-4} by measuring the distance of the beam paths in the third race track microtron of the MAMI accelerator. In the Saclay SATURNE experiment a high resolution, but small acceptance, spectrometer was used and, through an ingenious series of measurements on different nuclear reactions, the beam energy and spectrograph settings were both calibrated. The value of the η mass was then extracted from the missing-mass peak in the $p + d \to {}^3\text{He} + X$ reaction.

The BIG KARL spectrograph and the high brilliance beam at COSY are ideally suited to perform a high precision experiment in a self calibrating experiment. Three reaction products were measured at the same time with one setting of the spectrometer and one setting of the beam momentum. The reactions were

$$p + d \quad \to \quad t + \pi^+ \tag{1}$$
$$p + d \quad \to \quad \pi^+ + t \tag{2}$$
$$p + d \quad \to \quad {}^3\text{He} + \eta \tag{3}$$

It was always the first particle produced which was measured. Input are the well known masses of the proton, deuteron, π^+, triton and ^{3}He. For a beam momentum close to 1641 MeV/c all three particles are within the acceptance of the spectrograph. The pion is used to deduce the absolute beam momentum. Then the triton is used to fix the spectrograph setting and finally from the ^{3}He one obtains the mass of the η meson. In the analysis the target thickness, as measured from the triton momentum, was studied as function of measuring time. It was found that it increased with time most probably due to freezing out of air.

This is shown in the upper part of Fig. 1 which displays the variation of the target thickness as deduced from the measurement of tritons (Reaction 1). The lower part
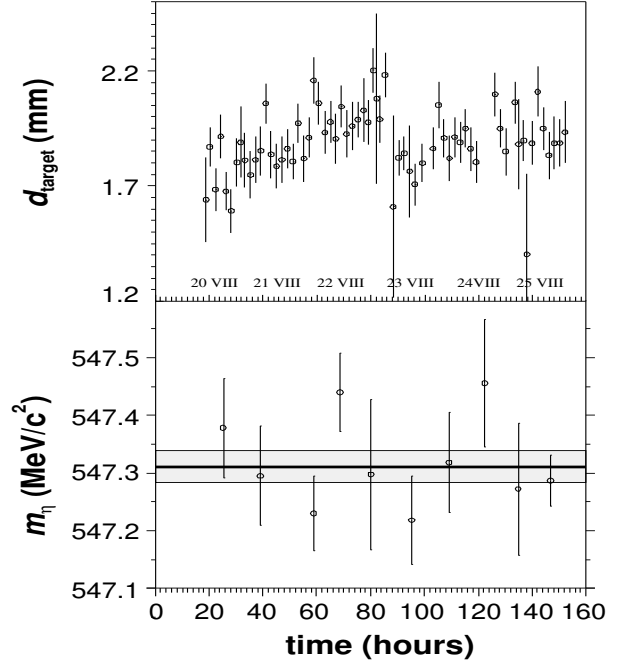

Fig. 1: Upper part: variation of the target thickness with time as deduced from the triton momenta. Lower part: same as above but for values of the η mass as deduced from the measured ^{3}He measurements. The thick line is the statistical mean value and the thin lines indicate the $\pm 1\sigma$ band.

shows the value of the η mass as deduced from the detected ^{3}He ions (Reaction 3). A thinner target at approximately the middle of the beam time coincides with a cleaning of the target windows. In order to investigate the properties of the spectrograph a series of calibration runs were performed. These include sweeping with the primary beam over the focal plane without a target at a beam momentum of 793 MeV/c. This corresponds to a reaction $p + 0 \to p + 0$. Then the full kinematic ellipse of deuterons from the reaction $p + p \to d + \pi^+$ at the same beam momentum was measured. Finally, pions from the reaction $p + p \to \pi^+ + d$ were measured at 1640 MeV/c, again sweeping the deuteron loci over the whole focal plane. Then the following procedure was adopted. It is assumed that the spectrograph is known. The three calibration reactions were now used to fix the beam momentum, the target thickness and the η mass. In a second step the assumption (known spectrograph) was studied by determining the missing mass of the unobserved particle in the calibration runs. These are the masses 0, π^+ and d. Deviations from PDG values have an uncertainty of $\sigma = \pm 28$ keV/c^2, which is the main contribution to the total systematical error of 32 keV/c^2. The missing mass measurement yields a statistical error of the same size.

The final result is:

$$m(\eta) = 547.311 \pm 0.028(\text{stat.}) \pm 0.032(\text{syst.})\,\text{MeV/c}^2 \ .$$

2

1.2.2 Evidence for an Excited Hyperon $Y^{0*}(1480)$

The reaction $pp \to pK^+Y$ has been studied at a beam momentum of 3.65 GeV/c at the ANKE spectrometer in order to investigate hyperon production. The missing mass spectra $MM(pK^+)$ have been analyzed and compared with extensive Monte Carlo simulations. A final state comprising a proton, a positively charged kaon, a pion of either charge together with an unidentified residue X was investigated in the reaction $pp \to pK^+Y \to pK^+\pi^{\pm}X^{\mp}$. In a first step of the analysis we have assumed that the measured missing mass $MM(pK^+)$ spectra can be explained by the production of well established hyperon resonances and non-resonant contributions. In Monte Carlo simulations the production of $(\Sigma^0(1385), \Lambda(1405)$ and $\Lambda(1520))$ and non-resonant contributions like $pp \to pK^+\pi X$ and $pp \to pK^+\pi\pi X$ — X denotes any hyperon which could be produced in the experiment — was included. The comparison of measured and simulated missing mass distributions shows a necessity to include an additional excited hyperon Y^{0*} with a (fitted) mass of $M(Y^{0*}) = (1480 \pm 15)$ MeV/c^2 and width $\Gamma(Y^{0*}) = (60 \pm 15)$ MeV/c^2, see Fig. 2.
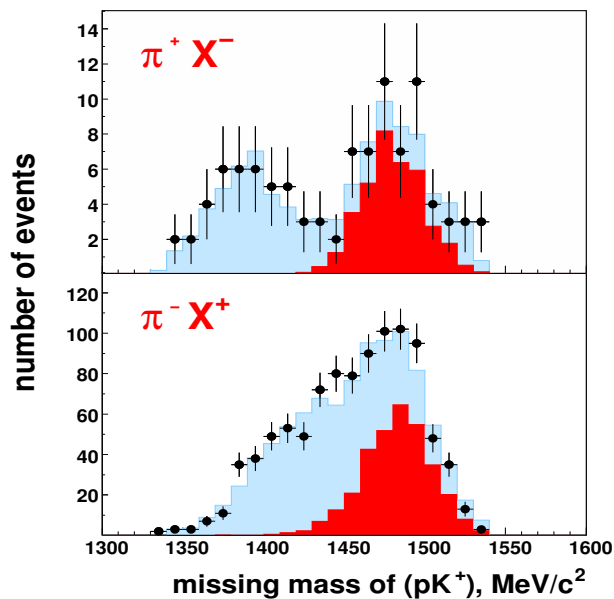

Fig. 2: Missing-mass $MM(pK^+)$ spectra for the reaction $pp \to pK^+\pi^+X^-$(upper) and $pp \to pK^+\pi^-X^+$(lower). Experimental data points with statistical errors are compared to the fitted overall Monte-Carlo simulations (shaded histogram, blue). The contribution from the Y^{0*} resonance with a mass of $M(Y^{0*}) = (1480 \pm 15)$ MeV/c^2 and a width $\Gamma(Y^{0*}) = (60 \pm 15)$ MeV/c^2 is shown as a solid (red) histogram.

The production cross section of the Y^{0*} is of the order of few hundred nanobarns. Since the Y^{0*} hyperon is neutral, it can be either a Λ or Σ^0 hyperon. On the basis of available data we cannot decide whether it is a 3-quark baryon or an exotic state. However, it seems to be difficult to validate that a $Y^{0*}(1480)$ hyperon is a 3q-baryon.

1.2.3 Investigation of scalar resonances $a_0/f_0(980)$

Fundamental properties of the scalar resonances $a_0/f_0(980)$, like their masses, widths and couplings to $K\bar{K}$, are poorly known. In particular, precise knowledge of the latter quantity would be of great importance since it can be related to the $K\bar{K}$ content of these resonances. a_0/f_0 production is studied at COSY in pp, pn and dd interactions, via their strange ($K\bar{K}$) and the nonstrange ($\pi\eta/\pi\pi$) decays. The first channel can be measured with ANKE, while for the second the WASA detector, which will be available for measurements in 2007, can be used. As a first step, isovector $K\bar{K}$ production has been measured in the reaction $pp \to dK^+\bar{K}^0$ at excess energies $Q_{K\bar{K}} = 46$ and 105 MeV. The analysis for the higher energy has now been finalized. At this energy, the acceptance of ANKE does not cover full phase space and, therefore, a model-independent acceptance correction is not possible. Instead, the coefficients in the transition matrix element (assuming that only S- and P-waves contribute) have been extracted from uncorrected spectra, using the ANKE-GEANT simulation programm, and used later for the acceptance correction of mass spectra and angular distributions. As an example for the acceptance corrected differential spectra, Fig. 3 shows the $K\bar{K}$ (a) and $d\bar{K}$ (b) invariant mass distributions.
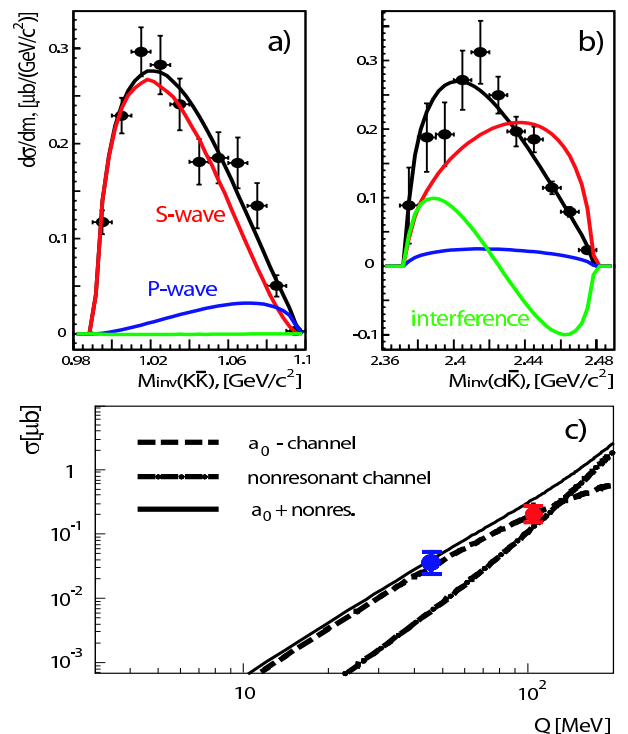
Fig. 3: $K\bar{K}$ (a) and $d\bar{K}$ (b) invariant mass distributions for the reaction $pp \to dK^+\bar{K}^0$ at $Q = 105$ MeV. The lines denote a partial wave decomposition with the $K\bar{K}$ pair in a relative S- and P-wave, respectively. Total cross section (c) as a function of Q in comparison with theoretical predictions for a_0^+ production and non-resonant background.

After kinematic fitting, the mass resolution for the $K\bar{K}$

spectrum is about 3 MeV over the full mass range. Also shown in the figure are the contributions from the *S*-wave, *P*-wave and interference terms of the matrix element. Angular distributions have also been deduced and included in the analysis.

The partial wave decomposition reveals *S*-wave dominance (more than 85%) for the both excess energies. Thus for excess energies below ~ 100 MeV $K\bar{K}$ production is mainly through the resonant (a_0^+) channel. The total cross section of the reaction $pp \rightarrow dK^+\bar{K}^0$ for $Q = 105$ MeV is $190 \pm 3_{stat} \pm 40_{sys}$. This value, as well as the contributions from the different partial waves, is in good agreement with theoretical predictions based on the Quark-Gluon-Strings Model, see Fig. 3.

1.2.4 Vector Meson Production

The $pp \rightarrow pp\phi$ reaction has been measured at ANKE for three different c.m. excess energies close to threshold, detecting the K^+K^- decay mode of the ϕ-meson. Figure 4 shows the total cross sections at $\varepsilon = 18.5$, 34.5 and 75.9 MeV together with the data point from DISTO ($\varepsilon = 83$ MeV). The dashed line is normalized to the ANKE data point at 75.9 MeV and corresponds to the energy dependence following phase-space. The solid line — normalized to all three ANKE data points — takes into account the effect of final-state interaction between the two protons in a $^1S_0$ state by the Jost function method. This simple approach describes the ANKE data. Analysis of the differential distributions at $\varepsilon=18.5$ MeV shows a dominant contribution of *s*-wave ϕ-mesons with the proton transition $^3P_1 \rightarrow {}^1S_0$. A clear effect of the proton-proton final-state interaction is seen from the proton-momentum distribution in the proton-proton reference frame.
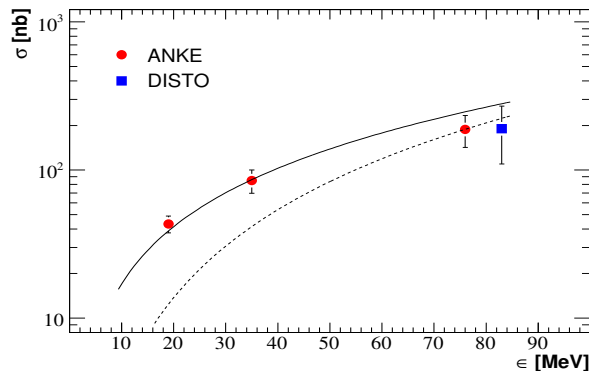

Fig. 4: Total cross section for ϕ-meson production in pp collisions as a function of the excess energy ε. The error bars include both statistical and systematic uncertainties. The dashed line shows a phase-space calculation, fixed to the high energy ANKE result, while the solid line includes proton-proton final-state interaction and is normalized to fit all ANKE data.

The Okubo-Zweig-Iizuka (OZI) rule states that processes with disconnected quark lines in the initial and final states are suppressed. Accordingly, the production of ϕ-mesons

from initial non-strange states is expected to be substantially suppressed relative to ω-meson production. The cross-section ratio for ϕ- and ω-meson production under similar kinematical conditions should then be in the order of $R_{OZI}=\sigma_\phi/\sigma_\omega=\tan^2\alpha_V=4.2\times10^{-3}$ where $\alpha_V=3.7°$ is the deviation from the ideal ϕ-ω mixing angle. Data from πN interactions as well as from mesonic and radiative decays indicate a ϕ-to-ω ratio of $3\times R_{OZI}$.

So far, the total ϕ cross section has been measured in pp collisions at only two energies in the range $\varepsilon=2$–4 GeV. The ϕ-to-ω ratio at these high energies agrees with the ratios from πN interaction and decay investigations. Using the DISTO result for $\varepsilon=83$ MeV, together with SPESIII and COSY-TOF data on ω-production, the ϕ-to-ω cross-section ratio can be calculated. This ratio is 7 times larger than R_{OZI}. The new ANKE results confirm the enhanced ϕ-to-ω ratio at $\varepsilon \sim 80$ MeV and show, within the existing uncertainties, a similar enhancement at 18.5 MeV and 34.5 excess energy. The weighted mean value for the ϕ-to-ω production ratio in the energy range from 18.5 to 75.9 MeV results in

$$R(\phi/\omega) = (3.3 \pm 0.6) \cdot 10^{-2}$$
$$R(\phi/\omega)/R_{OZI} = 7.9 \pm 1.4 .$$

However, the interpretation of the ϕ-to-ω ratio is ambiguous due to a poor knowledge of the production mechanisms even in case of the $pp \rightarrow pp\omega$ reaction. Therefore, in a 1-day evaluation measurement at ANKE about 9000 $pp \rightarrow pp\omega$ events have been taken at excess energies of 60 MeV and 92 MeV. The latter corresponds to the lowest energy measured at COSY-TOF while the SPES-III data have been taken below 31 MeV. Having both protons detected at ANKE the ω-meson is identified by the missing mass method. The separation of the $pp \rightarrow pp\omega$ events from a large $pp \rightarrow ppX$ background was found to be possible using kinematical transformations as a model-independent approach. It was also tested to obtain the differential cross sections as function of the ω center-of-mass angle Θ_{cm}^ω and the relative kinetic energy $\varepsilon(pp)$ of the two final-state protons presented in Fig. 5.

In average the measured distributions do not significantly deviate from the results of a phase space simulation. Still there is some systematics which can be related to the background subtraction procedure and needs further investigation. Assuming a pure phase-space distribution and not taking into account the final-state interaction of the 2-proton system, the analysis leads to a total cross-section of $\sigma_{tot}(Q = 60 \text{ MeV}) = 5\,\mu\text{barn} \pm 30\%$ and $\sigma_{tot}(Q = 92 \text{ MeV}) = 10\,\mu\text{barn} \pm 20\%$.

Due to the trigger conditions in this experiment the obtained data are neither sensitive to the final-state interaction of the two protons nor to their relative angular dependence. Small relative kinetic energies $\varepsilon(pp)$ are suppressed. For the same reason the extraction of the relative angular distribution of the two protons is not possible. For the actual data sample this introduces an additional systematic uncertainty as large as 50% to the total cross section. This can be significantly improved either in a
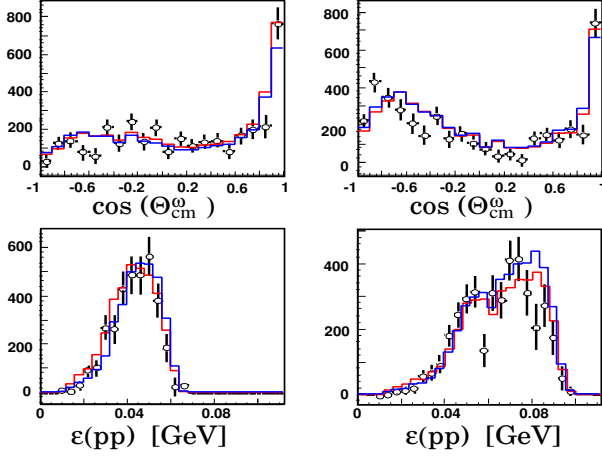
Fig. 5: Differential distributions of $pp \to pp\omega$ events along the the ω center-of-mass angle Θ_{cm}^{ω} and along the relative kinetic energy $\varepsilon(pp)$ of two protons obtained at Q=60 MeV (left column) and at Q=92 MeV. Phase-space simulations assuming an isotropic angular distribution of the two protons are shown by red lines. The blue lines correspond to a $\cos^2(\Theta_{cm}^{pp})$ angular dependence.

future experiment at ANKE getting additional information on the two proton state or by extracting the relative protons distributions from the COSY-TOF data.

1.2.5 The Charge-Exchange Reaction $\vec{d}p \to (pp)n$

One major feature of the polarised deuteron charge-exchange break-up reaction $\vec{d}p \to (pp)n$ is that the differential cross section and the two deuteron Cartesian analysing powers A_{xx} and A_{yy} are directly related to the magnitudes of the spin-spin neutron-proton charge-exchange amplitudes, which govern the spin-transfer observables in $\vec{n}p \to \vec{p}n$ at small momentum transfers. This raises the possibility of using the reaction to supplement the pn data base above 800 MeV per nucleon, where accurate polarisation data are more sparse.

A first measurement was carried out at ANKE with a 1170 MeV polarised deuteron beam. Having determined their vector and tensor polarisations before and during the acceleration of deuterons in the COSY ring, measurements of three tensor and two vector analysing powers showed that any depolarisation of the circulating beam is definitely less than 2%. The vector and tensor polarisations are typically about 74% and 59% respectively of the ideal values that could be provided by the polarised source.

The results for the two $\vec{d}p \to (pp)n$ tensor analysing powers are shown in Fig. 6 in 20 MeV/c bins in q for two cuts in the excitation energy, *viz.* $0 < E_{pp} < 1$ MeV and $1 < E_{pp} < 3$ MeV. In contrast to the strong and rapidly varying tensor analysing powers shown there, the vector A_y is consistent with zero for all momentum transfers.

For low excitation energy E_{pp} of the final pp pair, and small momentum transfers q, the $\vec{d}p \to (pp)n$ reaction
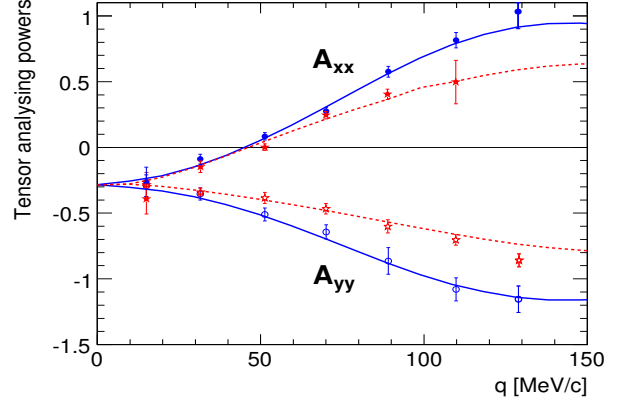

Fig. 6: Values of the tensor analysing powers A_{yy} and A_{xx} extracted for the $dp \to (pp)n$ reaction for $0 < E_{pp} < 1$ MeV (circles) and $1 < E_{pp} < 3$ MeV (stars). The curves correspond to the predictions of the impulse approximation program, for which the input amplitudes at 585 MeV were taken from SAID; $0 < E_{pp} < 1$ MeV (solid) and $1 < E_{pp} < 3$ MeV (broken).

mainly excites the $^1S_0$ state of the final pp system. This involves a spin-flip from the pn triplet to pp singlet and thus provides a *spin-filter* mechanism. In single-scattering approximation, the results depend only upon the np spin-dependent amplitudes β, γ, δ and ε. If we neglect the deuteron D-state, we expect that at low E_{pp}

$$
\begin{aligned}
A_{xx} &= \frac{|\beta|^2 + |\gamma|^2 + |\varepsilon|^2 - 2|\delta|^2}{|\beta|^2 + |\gamma|^2 + |\delta|^2 + |\varepsilon|^2}, \\
A_{yy} &= \frac{|\delta|^2 + |\varepsilon|^2 - 2|\beta|^2 - 2|\gamma|^2}{|\beta|^2 + |\gamma|^2 + |\delta|^2 + |\varepsilon|^2}, \\
A_y &= 0.
\end{aligned} \tag{4}
$$

Since in the forward direction $\beta = \delta$ and $\gamma = 0$, at $q = 0$ the value of $A_{xx} = A_{yy}$ depends only on the ratio of $|\beta|$ to $|\varepsilon|$, which changes smoothly with energy. However, the δ amplitude, which contains the one-pion-exchange pole, varies very rapidly with momentum transfer and almost vanishes when $q \approx m_\pi$. Hence A_{xx} should approach its kinematical limit of +1 in this region, and this is consistent with the trend of the data shown in Fig. 6.

The spin-triplet final states generally produce the opposite signs for the analysing powers to the singlet and so, as soon as one departs from the very small E_{pp} limit, a dilution of the A_{xx} and A_{yy} signal is predicted. This effect depends sensitively upon the final state interactions in the low energy pp system. These, together with the Paris-potential $S+D$-state deuteron wave function, are included in our full analysis program

The predictions of Fig. 6 used amplitudes from the current SAID NN phase shift solution. All the features of both A_{xx} and A_{yy} are reproduced for $q \leq 120$ MeV/c. Quantitative agreement with predictions based upon an up-to-date phase-shift analysis will allow one to use the charge-exchange data from ANKE for pn studies in more barren regions.

5

1.2.6 Investigation of the ^{3}He $-\eta$ interaction

For studies of the ^{3}He-η interaction dp collisions are very well suited due to the relatively high cross sections for the $dp \to\, ^3$He η reaction and due to much better beam momentum definition compared to the $\gamma\,^3$He $\to\, ^3$He η and $\pi^+\,^3$H $\to\, ^3$He η measurements. Of interest are experiments both above and below the η production threshold. In the first case low energy ^{3}He-η scattering parameters can be determined on the basis of FSI effects. In the later case one can search for resonance-like structures originating from decays of a possible ^{3}He-η bound state, *e.g.* into the $dp \to\, ^3$He π^0 channel.
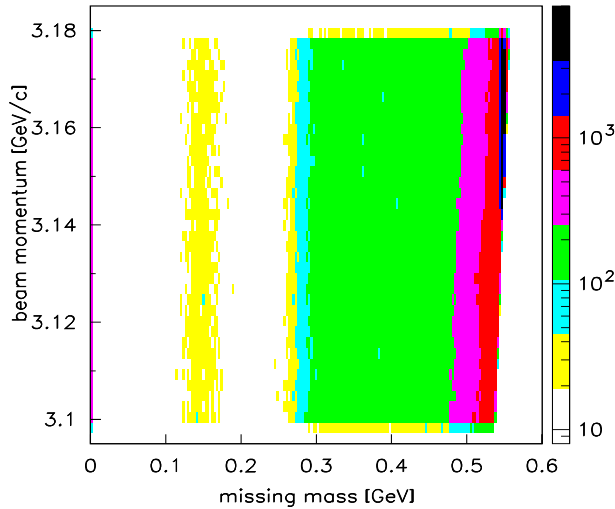

Fig. 7: Missing mass as a function of beam momentum. The onset of the η production is clearly seen the missing mass of 0.547 GeV and the threshold momentum of 3.141 GeV/c.

We performed measurements of the $dp \to\, ^3$He$X, X = \pi^0, \eta$ reactions near the η threshold using a slowly ramped deuteron beam of COSY scattered on a proton target. The momentum of the deuteron beam was varied continuously within each cycle from 3.095 GeV/c to 3.180 GeV/c, crossing the threshold for the $dp \to\, ^3$He η reaction at 3.141 GeV/c. The ^{3}He ejectiles were registered with the COSY-11 detection setup. In the missing mass spectrum determined as a function of the beam momentum (see Fig. 7) a clear signal from the η meson production as well as from the single π^0 production is visible. The ongoing data analysis indicates that the collected data will allow to determine the total and differential cross sections for the $dp \to\, ^3$Heη reaction with a high statistical accuracy on the level of 1%. A preliminary excitation curve for the pion production in the reaction $dp \to\, ^3$He π^0 shows no structures which could originate from decays of ^{3}He $-\eta$ bound state.

1.3 Status of experimental facilities

1.3.1 ANKE

Since summer 2005 ANKE is equipped with a polarized internal target (PIT) between the magnets D1 and D2, see Fig. 8. With an atomic beam source (ABS) polarized beams of hydrogen or deuterium atoms with an intensity of $7 \cdot 10^{16}$ atoms/s and a polarization of more than 90% is produced. This beam can be used as a jet target or be stored in a T-shape storage cell to increase the target density up to $5 \cdot 10^{13}$ cm^{-2}. The polarization of the target atoms will be measured with a Lamb-shift polarimeter.
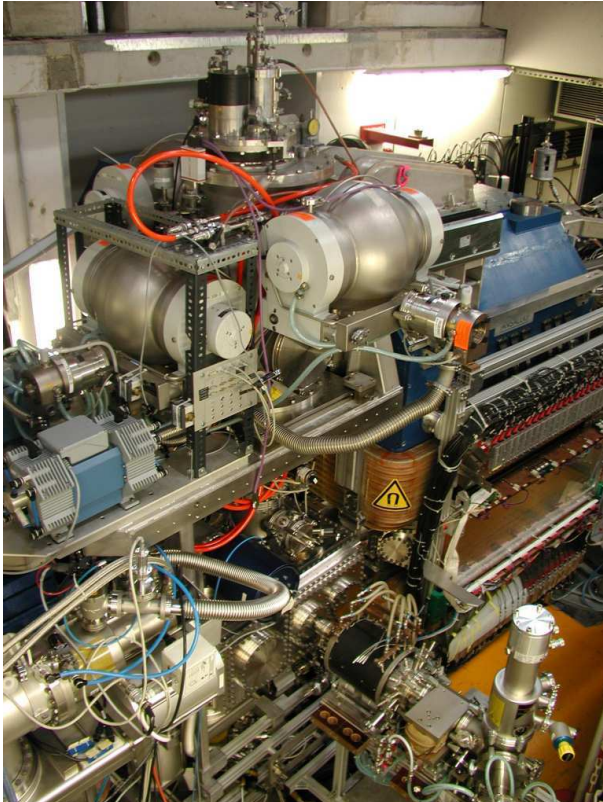

Fig. 8: Photo of ANKE with the polarized target in front of the spectrometer dipole D2 (blue). Components of the Lamb-shift polarimeter are on the right side of the ANKE target chamber.

1.3.2 COSY-TOF

End of 2004 COSY-TOF performed a beam time with the goal to obtain decisive information on the existence or non-existence of the exotic Θ^+ state where the situation is still confusing. The goal of this run is to investigate the significance of the previously found signature for the pentaquark Θ^+ in the $K^0 p$ system via the reaction $pp \rightarrow \Sigma^+ K^0 p$ (COSY-TOF collaboration, Phys. Lett. B **595**, 127 (2004)). To improve the statistical accuracy significantly, in addition to the higher luminosity, the detector was upgraded by a three layer Sci-Fi-hodoscope. The new data are estimated to contain a factor of 5 more statistics compared to the previous measurement.

The analysis is being performed by different collaboration groups separately. In this way, the investigation of the $pp \rightarrow \Sigma^+ K^0 p$ and especially the $K^0 p$ invariant mass will be approached independently on three different ways. Minimal cuts will be applied in order to observe control channels like the elastic scattering and the related reaction $pp \rightarrow \Lambda K^+ p$. The study and interpretation of the reaction $pp \rightarrow \Sigma^+ K^0 p$ and the $K^0 p$ mass spectrum will be approached only after comparison of the control channel results including dedicated simulations and without further tuning of the analysis software. In this context also the Dalitz plot, which is fully covered in our experiment, will be of decisive importance.

It is internationally agreed upon that the new COSY measurement will have crucial impact on the clarification of the situation.

1.3.3 Transfer of the WASA Detector

The transfer of the WASA detector from CELSIUS to COSY has been finished in September 2005. The components are presently being tested and prepared for installation at COSY scheduled for summer 2006. Commissioning is anticipated for the second half of 2006, allowing a start of the physics program (for details — on both the experimental program and the detector setup and performance — we refer to the "WASA-at-COSY" proposal nucl-ex/0411038) beginning of 2007 as orignially scheduled.

Pellet Target

After transfer and after maintenance of pumps and cryogenic equipment the WASA pellet target has been set up at COSY for a full scale test operation with access to all components prior to installation at COSY (Fig. 9).

The test program aims at reproducing the reliable target performance with hydrogen and an improved operation with deuterium. Only minor modifications are planned before installation, constructional changes are intended to reduce vibrations at the pellet generator to minimize the geometrical spread of the pellet beam and, consequently, the gas load.

The technology for the manufacturing of glass nozzles and vacuum injection capillaries has been transferred to the Central Department of Technology (ZAT) of the Research Centre Jülich, and preparations for production are ongoing. The VME interfaced SIMATIC slow control system remains unchanged compared to operation at CELSIUS, the stand–alone version to be used at COSY was already tested before dismount at CELSIUS.

In the future it is foreseen to extend the beam dump by 300 mm to improve access for maintenance and to provide space for a pellet tracking system.

Central Detector

The central detector setup will remain unchanged to the

Fig. 9: Test setup of the WASA pellet target at COSY with pellet generator (top), a dummy vacuum chamber around the nominal interaction zone, and pellet beam dump (bottom).

WASA setup at CELSIUS for installation and commissioning.

The CsI(Na) crystals of the scintillating electromagnetic calorimeter have already been tested after the transfer to COSY; no transport damage has been found. During the tests until installation the hydrophilic crystals are kept in a specially built air–conditioned measurement cabin with a level of humidity below 35 % (Fig. 10).

After installation, a corresponding closed atmosphere will be ensured by a tent. Presently, the Hamamatsu 1924 phototubes used in the forward part of the calorimeter are being replaced by an upgraded version 1924A with a significantly improved linearity.

The cryogenic cooling plant for the solenoid operation has already been assembled (Fig. 10). It will be set into operation beginning of 2006, with the solenoid due to be tested before installation at COSY.

The central drift chamber (MDC) — as well as the forward proportional straw chamber (FPC) — are presently operated under laboratory conditions to further optimize systematically the working point in view of gas mixture and high voltage supply. Frontend electronics have been completely exchanged for both straw detectors tak-
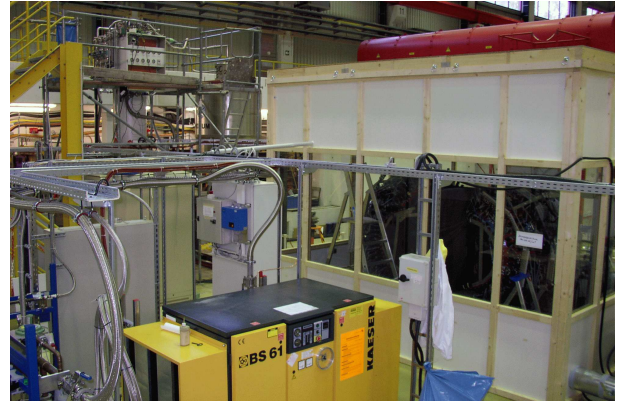

Fig. 10: The half spheres of the scintillating electromagnetic calorimeter in an air-conditioned cabin (back) and components of the cryogenic plant after setup for operation (front) in the COSY interior area.

ing over the solution for the straw detectors at the ANKE experiment based on the CMP16 amplifier-discriminator chip originally developed for the CERN CMS experiment. A complete system consisting of detectors, analog and digitizing electronics will be tested in the laboratory prior to installation. Due to both the limited time available and the risk of collateral damage individual non-working straws (few per cent) will not be repaired. Instead, also with respect to possible aging effects, it is foreseen to build a spare MDC from already existing hardware as soon as possible and to replace the detector. At a later stage it is planned to increase the position accuracy and efficiency of the central detector in its very forward region for measurements at higher energies by a scintillating fibre detector replacing the forward part of the plastic barrel scintillator in combination with additional dE information.

Forward Detector

For an efficient tagging at the higher energies available at COSY compared to CELSIUS, the WASA forward detector has to be upgraded prior to installation. During this first phase, the dE–E information provided by the Forward Range Hodoscope (FRH) will be improved by adding an additional layer of scintillator material, improving the precision of the energy information for protons with kinetic energies close to 1 GeV by 25 % compared to the present setup. The design of the additional detector component is finished and photomultiplier tests are presently performed.

A fourth existing straw chamber plane of the FPC will be installed and the setup of planes will be rearranged to increase the lever arm for track reconstruction resulting in an improved vertex reconstruction at the interaction point. Extra space available at COSY compared to CELSIUS allows for these modifications. Furthermore, a Cerenkov detector will be added in front of the Forward Range Hodoscope as soon as possible after

the commissioning phase to improve both the energy resolution for measurements at higher energies and particle identification.

Data Acquisition

Since the existing WASA data acquisition system (DAQ) is both not fast enough for the expected event rates and the digitizing Fastbus hardware is not serviced any more, a new DAQ system allowing event rates in the order of 10 kHz has been designed for WASA at COSY. The acquisition system will be compatible with existing systems at other COSY experiments, which allows to take over common electronic parts and most of the software. In addition, on-site maintenance will be provided by staff of the FZJ Central Institute for Electronics (ZEL). To meet the requirements of WASA-at-COSY new digitization modules are presently being developed: Slow and fast TDCs for straw and scintillation detectors, and slow and fast QDCs for the scintillating electromagnetic calorimeter and the plastic scintillators, respectively. The latter are realized as continuosly running flash ADCs with extensive FPGA processing for time stamping, integration, as well as pileup detection and possible correction. TDC prototypes are already available, and the QDC, a common development of ZEL and Uppsala University, is in the prototyping phase. Mass production is expected to be finished in time for commissioning in the second half of 2006.

Mechanical Preparation

Preparations at the internal target location, i.e. the necessary concrete work, and rearrangement of power and water supply lines, have been finished. An adjustment of the original detector mainframe in height for usage at COSY is under manufacturing, a test installation is planned for January 2006. A rail system for the central detector is already installed inside the COSY tunnel, and the carriages for the calorimeter are presently being modified. The original platform of the WASA forward detector can be reused. However, it has to be lifted by 285 mm to adapt for the difference in height of the beamline of COSY compared to CELSIUS. Platforms both to provide access to target components after installation and for the WASA trigger electronics will be finished for the COSY summer shutdown.

Collaboration

The WASA-at-COSY Collaboration has formally been constituted during a first collaboration meeting held in Jülich on November 4–5, 2005. At present the collaboration consists of 168 scientists from 27 institutes in seven countries.

For further information see the collaboration homepage `http://www.fz-juelich.de/ikp/wasa`.

2 External Experiments

2.1 Pionic Hydrogen at PSI

Pionic-atom data allow precision measurements of QCD quantities at the few-% level because no extrapolation or normalisation procedures must be applied. In pionic hydrogen (πH) the hadronic shift ε_{1s} and broadening Γ_{1s} of the atomic ground-state are related to the πN scattering lengths a^+ and a^- by Deser-type formulae: $\varepsilon_{1s} \propto (a^+ + a^-)$ and $\Gamma_{1s} \propto (a^-)^2$. The isoscalar quantity a^+ is connected to the πN σ-term which is a measure of chiral symmetry breaking, and the isovector part a^- yields the πN coupling constant.

K X-ray transitions in πH have energies around $3\,\text{keV}$ whereas ε_{1s} and Γ_{1s} are 7 and 1 eV, respectively. Thus, precision data can be achieved only with crystal spectrometers. The shift, now being determined to two per mille, exceeds the theoretical accuracy. In order to achieve also for Γ_{1s} an uncertainty comparable to theory, due to the complexness of πH ground-state transitions, new experimental approaches had to be applied.

Contributions to the X-ray line shape are (i) a Lorentzian due to the life time of the atomic levels (Γ_{1s}), (ii) the spectrometer response, and (iii) Doppler broadening. The latter stems from acceleration of the πH system in collisions with H_2 molecules during the atomic cascade where the de-excitation energy of various transitions $n \to n'$ is converted into kinetic energy (Coulomb de-excitation).

Hence, a precision determination of Γ_{1s} requires,
- ultimate knowledge of the spectrometer response,
- correction for the Doppler broadening,
- high statistics in the πH X-ray spectra, and
- good control of the background.

The spectrometer response was obtained with the narrow M1 transitions in helium-like sulphur, chlorine, and argon having energies close to the πH Kα, Kβ, and Kγ lines. For that an electron-cyclotron resonance ion trap (ECRIT) was set up providing sufficiently high count rates. The spectra of the various charge states make obvious the complex dynamics of few-electron systems measured here with unprecedented resolution (Fig. 11).

A measurement of the Kβ line in μH revealed nicely various Doppler contributions, because here the X-ray line shape is determined only by the (well known) spectrometer response and Coulomb de-excitation. The atomic cascade is now understood well enough for a reliable correction of the Doppler broadening. A low background level was achieved by a dedicated concrete shielding and the use of charge-coupled devices for X-ray detection.
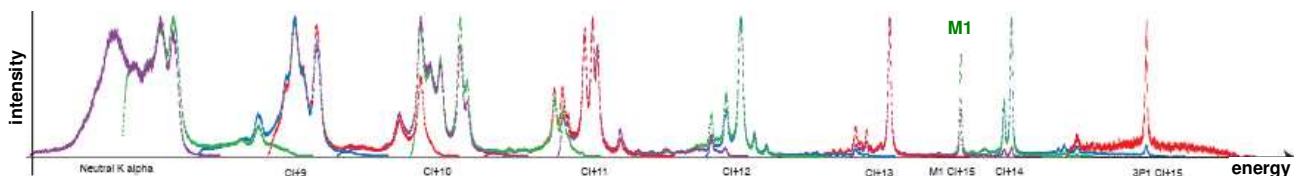
Substantial progress has been achieved relating ε_{1s} and Γ_{1s} to a^+ and a^- within the frame work of chiral perturbation theory (χPT). Theoretical uncertainties for ε_{1s} and Γ_{1s} are 2.9% and 0.2% obtained in 3rd order calculations. The new πH data, $\varepsilon_{1s} = 7116 \pm 11$ meV ($\pm 0.2\%$) and $\Gamma_{1s} = 785 \pm 27$ meV ($\pm 3.5\%$), yield values for $a^\pm$ as shown in Fig. 12 (πH: χPT+IB).

It has been reported recently, that for pionic deuterium (πD) the inclusion of isospin-breaking effects (IB) is of outstanding importance due to cancellations of the $\pi^- p$ and $\pi^- n$ interactions. In particular, the value of a^+ determined from ε_{1s} in πD is then no longer in striking disagreement with πH data. A 2nd order χPT calculation including IB, based on the recent πH measurement and $\varepsilon_{1s}^{\pi D} = -2.47 \pm 0.06\,\text{eV}\,(\pm 2\%)$ obtained earlier (πH+πD: χPT+IB), is shown together with the πH analyses (Fig. 12). Without IB effects (πH+πD: χPT), the result is far off as are the results of the previous experiment analysed in a potential approach.

$\Gamma_{1s}^{\pi D}$ is directly related to the threshold parameter α in pion production. At present, πD atom and $pp \to \pi^+ d$ production data disagree by 2 standard deviations.
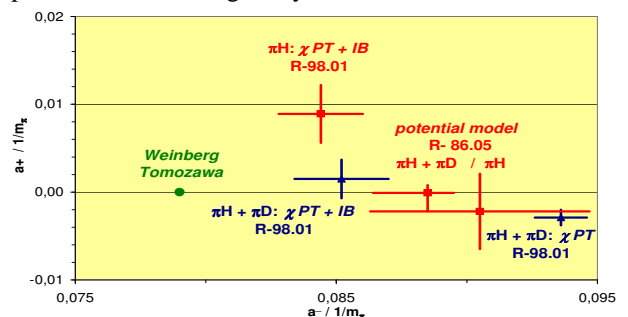
Fig. 12: Isoscalar *vs.* isovector scattering lengths a^+ and a^- as obtained from this (R-98.01) and previous experiments (R-86.05). Current algebra (Weinberg-Tomozawa point) gives the leading order in ChiPT.

A re-determination of $\varepsilon_{1s}^{\pi D}$ with a precision comparable to hydrogen, together with a combined πH + πD analysis, will improve the constraints for the πN scattering lengths a^+ and a^- and, consequently, for the πN σ-term and the πN coupling constant. From $\Gamma_{1s}^{\pi D}$, an accuracy for α will be achievable being a factor of 2-3 better than in pion production experiments.

The experimental program for πH has been completed end of 2005 with a high-statistics measurement of the πH Kα transition at the πE5 beam line of PSI. From these data finally an uncertainty of less than 2% is expected for Γ_{1s} in πH. A precision determination of the strong-interaction effects in πD is planned for 2006.

Fig. 11: X-rays from chlorine charge states excited in the ECRIT. The crystal spectrometer resolution for the πH Kβ line (2.886 keV) is obtained from the M1 transition (2.757 keV) in the helium-like ion Cl^{15+}.

3 Theoretical Investigations

The IKP theory group studies the strong interactions in their various settings — spanning topics ranging from hadron structure and dynamics to the nuclear many-body problem. The main focus is on the formulation and application of effective field theories for precision hadron and nuclear physics based on the symmetries of Quantum Chromodynamics. Some of the high-lights of these activities are discussed in the following.

3.1 Effective field theory for pion production in proton-proton collisions

With the appearance of high quality data for the reactions $NN \rightarrow NN\pi$ in the early 90ties it became evident that the dynamics of this class of reactions is not at all understood: the existing models failed to describe the data by a factor of about 10 for the reaction $pp \rightarrow pp\pi^0$ and by a factor of 2 for $pp \rightarrow d\pi^+$. In the following years several proposals were put forward, especially to explain the huge discrepancy in the neutral pion production channel. It was shown that these data could be described either by heavy meson exchanges, (off-shell) pion rescattering, or pion emission from exchanged mesons. To resolve the confusion various groups started to investigate $NN \rightarrow NN\pi$ using chiral perturbation theory (ChPT). As an effective field theory it is to be free of any ambiguities and one expected that now the relevant physics of $NN \rightarrow NN\pi$ could be identified. As a big surprise to many, however, it turned out that, when naively using the original power counting by Weinberg, the discrepancy between theory and data became even larger at next-to-leading order (NLO) for $pp \rightarrow pp\pi^0$ as well as for $pp \rightarrow d\pi^+$. In parallel it was realized that the large momentum transfer characteristic for meson production in NN collisions calls for a modification of the counting scheme. When applied to p-wave pion production evidence was found for a convergence of this scheme towards the data. For s-wave production so far only preparatory work was available — especially there was no calculation that included both the final and initial state interaction. It was thus a significant progress when we succeeded this year to perform the first complete calculation up to NLO for $NN \rightarrow d\pi$, including the distortions from the NN interaction. In this work we could show that the sum of all loops that appears at NLO cancels an irreducible piece that emerged from the convolution of the leading pion rescattering operator with the one-pion-exchange contribution of the NN potential. The net effect of this was to replace the $\pi N \rightarrow \pi N$ subamplitude by its on-shell value — before it was a factor of 3/4 smaller due to the special kinematics of pion production. The result is shown in Fig. 13, where it can be seen that now the factor of 2 discrepancy of the original calculation is overcome. The theoretical uncertainty of the calculation is still significant (indicated in the figure by the box) but will be improved soon — a calculation up to NNLO is in preparation.
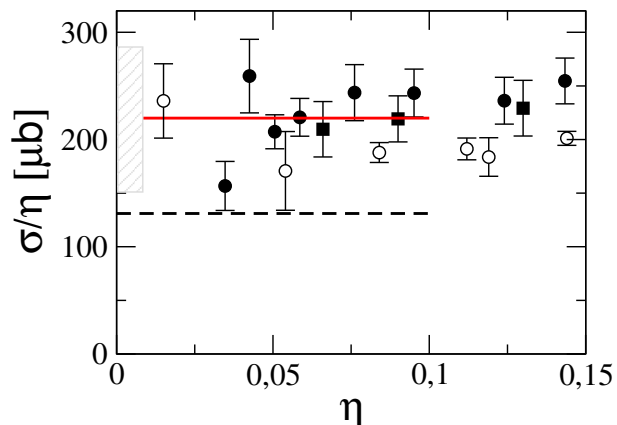

Fig. 13: Comparison of our results to experimental data for $NN \rightarrow d\pi$ where η is the pion momentum in units of the pion mass. The dashed curve show the LO result and the solid line shows the result at NLO. The estimated theoretical uncertainty at NLO is illustrated by the filled box. The data are from TRIUMF (Canada) and COSY.

It should be stressed that this result clearly shows the necessity to perform pion-production calculations within the controlled framework of an effective field theory for it turned out that all those mechanisms included in phenomenological calculations mentioned above can be mapped on amplitudes within ChPT that appear at NNLO. However, at this order there is at the same time a large number of loops. On the other hand the cancellations found in our work could never be observed in phenomenological calculations where typically only subgroups of diagrams, leading to individually significant contributions, were included.

3.2 Chiral extrapolations for lattice QCD

Lattice QCD is a tool to calculate baryon properties from first principles. However, at present, simulations can only be done for quark (pion) masses considerably above the physical values, typically $M_\pi > 400$ MeV in state-of-the-art calculations. Chiral perturbation theory is able to provide extrapolation functions that connect such lattice data with the realistic pion masses. We have started a systematic analysis of the quark mass dependence of various baryon properties derived from chiral perturbation theory. The quark mass dependence of an observable is encoded in loop and contact term contributions, the latter are accompanied by the so-called low-energy constants (LECs). There are two classes of low-energy constants. Class I LECs parameterize the quark mass effects whereas the dynamical LECs of class II are related to pion momenta (derivatives). Given the scarcity of precise and systematic lattice data, we consider it extremely important to utilize phenomenological input obtained from the analysis of many different processes to constrain the dynamical LECs. Of equal importance is the estimation of the ensuing theoretical uncertainty for

any given baryon observable, related to the uncertainties with which LECs from the mesonic and the baryon sector have been determined. Within this framework, we have analyzed many baryon observables like the nucleon and the baryon octet masses, the pion- and kaon-nucleon sigma terms, the isovector anomalous magnetic moment or the axial-vector coupling of the nucleon. These studies are based on complete one-loop representations. Incorporating only the leading loop effects that appear at third order, as it is often done, does not lead to a sufficient precision. In Fig. 14 we show such extrapolations for the nucleon mass based on the SU(3) representation with all dimension two LECs fixed from an earlier study of the octet masses. For pion masses >500 MeV, the theoretical uncertainty becomes very large — such a statement depends, however, on the observable considered.
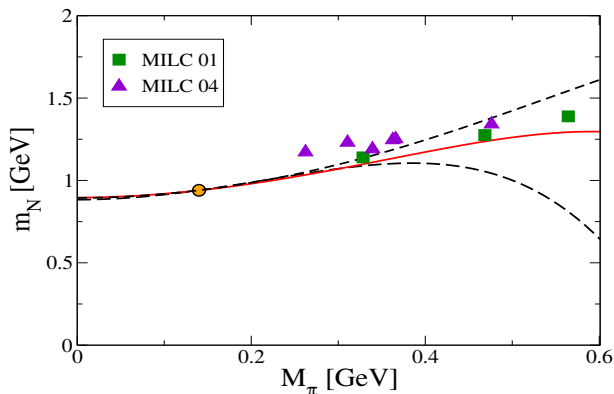

Fig. 14: Pion mass dependence of the nucleon mass in flavor SU(3). The red line gives the best fit and the black lines give the theoretical uncertainty under the constraint that the nucleon mass takes its physical value for the physical quark masses. Green squares: MILC 2001 data, purple triangles: MILC 2004 data.

It can be stated in general that using extrapolation functions based on a chiral perturbation theory representation cease to make sense at higher pion masses, say above 500 MeV. Note also that the most recent data from the MILC collaboration at the lowest pion masses can not be described, the source of this problem remains to be identified. The lattice community is therefore urgently asked to provide data at sufficiently small pion masses for a cornucopia of observables — otherwise a model-independent analysis of lattice results will not be possible. In the context of QCD, chiral perturbation theory is a faithful representation for the analysis of the Goldstone boson and the baryon octet properties. If one wants to consider also excited states (resonances), the construction of the corresponding effective field theories must respect resonance decoupling. We have constructed a covariant effective field theory for the delta resonance in which the nucleon-delta mass splitting is counted as an additional small parameter. Using this approach, we have calculated the delta mass, the delta-nucleon mass splitting and the pion-delta sigma term. We find that the nucleon-delta

splitting increases by about ten percent in the chiral limit and also, the pion-delta sigma term is sizeably smaller than the one of the nucleon, indicating strong violations of spin-flavor SU(4). We have also worked out extrapolation functions for the ρ-meson mass based on a formulation that extends infrared regularization to spin one fields.

3.3 Theory of spin filtering

The physics potential of experiments with high-energy stored polarized antiprotons is very large, and for more than two decades, physicists have tried to produce beams of polarized antiprotons without success. The list of fundamental issues accessible with polarized antiprotons includes the determination of transversity — the last leading-twist missing piece of the QCD description of the partonic structure of the nucleon — without measurements of which the spin tomography of the proton would ever be incomplete. Other items of great importance for the perturbative QCD description of the proton include the phase of the time-like form factors of the proton and hard proton-antiproton scattering. Such an ambitious physics program for a polarized antiproton-polarized proton collider has been proposed recently by the PAX Collaboration for the new Facility for Antiproton and Ion Research (FAIR) at GSI in Darmstadt. An integral part of such a machine is a dedicated large-acceptance Antiproton Polarizer Ring (APR). As a part of the theoretical support of the PAX proposal, the dynamics of the spin filtering of stored protons in a polarized internal target has been scrutinized, leading to novel insight into this phenomenon. The spin filtering in storage rings is based on a multiple passage of a stored beam through a polarized internal gas target. Apart from the polarization by spin-dependent transmission, a unique geometrical feature of the interaction with the target in such a filtering process is the scattering of stored particles within the beam. A depolarization effect in the scattering process affects the polarization build-up. In the Jülich theory group we derived the quantum-mechanical evolution equation for the spin-density matrix of a stored beam which incorporates the scattering within the beam. It describes the change of the interplay of the transmission and scattering-within-the-beam from polarized electrons to polarized protons in the atomic target. Specifically, a complete self-cancellation of the transmission and scattering-within-the-beam contributions from polarized electrons is found. The evaluation of corrections from the scattering within the beam of protons in the polarized targets requires a careful evaluation of the Coulomb-nuclear interference effect in the region of extremely small scattering angles inaccessible in direct experiments. The effect of the spin-flip scattering within the beam to the polarization cross section is proven to be negligible small. These results agree with those found by the Milstein-Strakhovenko group from the Budker Institute. There is only a slight disagreement between the recently reanalyzed FILTEX result for the po-

larization cross section, $\sigma_P = 72.5 \pm 5.8\,\text{mb}$, and the theoretical expectation $\sigma_P \approx 86\,\text{mb}$. Regarding the future of the PAX proposal, the conclusion is that one can only rely upon the nuclear antiproton-proton interaction and must optimize the filtering process using the antiprotons available elsewhere (CERN, Fermilab).

3.4 $p\bar{p}$ interactions in J/ψ decays

Recently the BES Collaboration reported a near-threshold enhancement in the proton-antiproton ($p\bar{p}$) invariant mass spectrum, observed in the $J/\Psi \to \gamma p\bar{p}$ decay. Signs for a low mass $p\bar{p}$ enhancement had been already seen earlier in low-statistics experiments, the new data from BES, however, are of rather high statistical accuracy and therefore provide very precise information about the magnitude and the energy dependence of the $p\bar{p}$ mass spectrum very close to threshold. The BES Collaboration fitted their $p\bar{p}$ invariant mass spectrum below 1.95 GeV by a Breit-Wigner resonance function. Assuming that the $p\bar{p}$ system is in an S-wave resulted in a resonance mass of $M = 1859^{+3+5}_{-10-25}$ MeV and a total width of $\Gamma < 30$ MeV. A comparable fit to the data could be achieved with a P-wave Breit-Wigner function with $M = 1876 \pm 0.9$ MeV and $\Gamma = 4.6 \pm 1.8$ MeV. The proximity of these resonance masses to the $p\bar{p}$ reaction threshold (which is at 1876.54 MeV) nourished speculations that the observed strong enhancement could be a signal of an $N\bar{N}$ bound state. While theoretical considerations of such $N\bar{N}$ bound states (or of baryonia, in general) abound in the literature, there is so far hardly any undisputed experimental information on the existence of such states. Thus, the assumption that one has found here independent and possibly even more convincing evidence in support of $N\bar{N}$ bound states is certainly appealing. In our investigation we showed that the observed enhancement could have also an entirely different and much more conventional interpretation. In particular, we argued that the enhancement is primarily due to the final-state interaction between the produced proton and antiproton. For this study we utilized a realistic model of the $N\bar{N}$ interaction. The elastic part of this model is the G-parity transform of the Bonn meson-exchange NN potential, supplemented by a phenomenological complex potential to account for $N\bar{N}$ annihilation. The $p\bar{p}$ mass spectrum from the decay $J/\Psi \to \gamma p\bar{p}$ measured by the BES collaboration is shown in Fig. 15. The blue line indicates the pure phase-space distribution, i.e. the result one expects for a reaction amplitude that has no energy dependence. The green curve is the squared scattering amplitude predicted by one of our $N\bar{N}$ models for the $^1S_0$ partial wave and the isospin $I = 0$ channel, suitably multiplied with phase-space factors in order to match it to the kinematics of the J/Ψ decay reaction. Finally, the red curve is the result of a calculation where we assume that the basic reaction amplitude is a constant but take into account the effects of the $p\bar{p}$ final-state interaction within the so-called Watson-Migdal approach. Obviously, those results are in remarkable agreement with the

experiments from the BES collaboration. We should add that the structure around invariant masses of $M(p\bar{p}) \approx$ 2.1 GeV is mostly likely due to the $f_0(2200)$ resonance, which was not included in our analysis. Note also that the structure at around 2.98 GeV is the well known η_c meson.
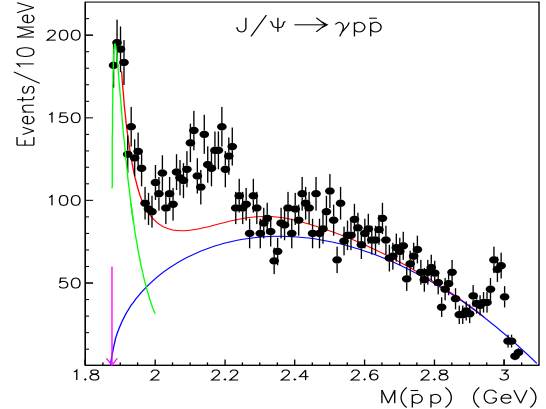

Fig. 15: The $p\bar{p}$ mass spectrum from the decay $J/\Psi \to \gamma p\bar{p}$. The arrow indicates the reaction threshold.

3.5 Spectra and binding energy predictions of chiral interactions for ^{7}Li

It is well known that the properties of nuclei cannot be well reproduced using todays very accurate two-nucleon (2N) interaction models only. It is generally accepted that additional forces, namely three-nucleon forces (3NFs), are required for an accurate description of nuclear binding energies and spectra. These interactions naturally arise in the framework of chiral perturbation theory. Their quantitative determination is essential to define the nuclear interaction completely for investigations of, e.g., the properties of unstable nuclei. At the same time, this provides an important test of our understanding of the nuclear forces, because it will confirm or disprove a tight relation of the 2N interaction, πN amplitudes and 3N forces, which is believed to be the consequence of the spontaneously-broken chiral symmetry of QCD. Because 3N scattering experiments can probe the 3NFs only in the isospin $T = 1/2$ channel, the p-shell nuclei provide an important additional laboratory, which enables us to study the interplay of $T = 1/2$ and $T = 3/2$ components of 3NFs. To this aim, we performed the first calculation of the spectra and binding energy of ^{7}Li based on chiral 2N and 3N interactions. The non-locality of the forces requires using the no-core shell model approach, leading to a high dimensional shell model calculation, which was performed on a massively parallel supercomputer. Two sets of parameters for the 3N forces describe the s-shell nuclei equally well. Therefore, we were able to study the sensitivity of the ^{7}Li system on the structure of the 3N force, keeping the description of the s-shell nuclei the same. Our results confirm this sensitivity for both, the binding energy and the excitation spectrum, see Fig. 16.

In no case, however, we find overbinding or unrealistically high densities in ^{7}Li, although the chiral interactions are much softer than the traditional forces. We also find slight deviations of our results from the experimental values, which suggest slight changes of the strength of 2π exchange in the NN and 3N force in order to describe the p-shell and s-shell nuclei simultaneously. A study of this conjecture is in progress. Also the extension to the more demanding mid-shell nuclei and to neutron-rich isotopes is a high priority and will finally allow to pin down the isospin dependence of the 3NF.
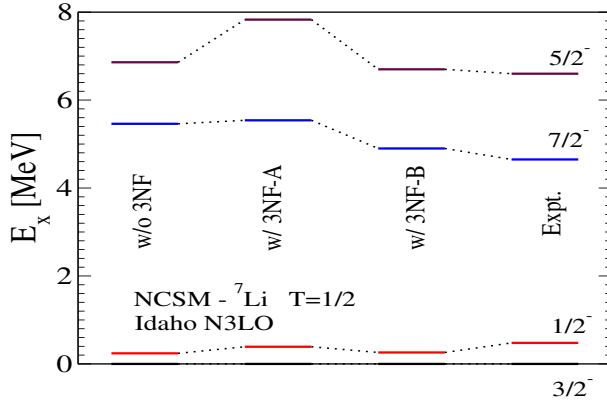
Fig. 16: Predictions for the excitation spectrum of ^{7}Li based on chiral *NN* forces alone and together with two choices for the chiral 3NF and the data.

3.6 Pygmy dipole resonances in Calcium isotopes

Soft electric dipole modes of nuclei, the so-called pygmy resonances, are relevant for the synthesis of many nuclei in supernova explosions. Last year, the electric dipole strength below 10 MeV has been measured in the nucleus ^{44}Ca with nuclear resonance fluorescence in Darmstadt. This nucleus is important as it allows to study the effect of pairing correlations which are negligible in the closed-shell nuclei ^{40}Ca and ^{48}Ca. Pairing correlations are crucial for the studies of radioactive nuclei.

The experimental isovector dipole sum rule exhaustion integrated up to 10 MeV shows a non-linear dependence on the neutron excess, see Fig. 17. The quasiparticle random-phase approximation (RPA), in contrast, produces a sum rule exhaustion which scales linearly with the neutron excess. This is due to the increasing occupation of the neutron $f_{\frac{7}{2}}$ level. Clearly, one has to go beyond the quasiparticle RPA. The extended theory of Finite Fermi Systems (ETFFS) which goes beyond the RPA by incorporating phonon degrees of freedom has been generalized to include pairing correlations (ETFFS(QTBA)). First numerical studies of the Ca isotopes have been performed, see Fig. 17.

The phonon coupling strongly fragments the strength. This leads to shifts of the electric dipole strength. In ^{48}Ca, some dipole strength is shifted to energies above 10 MeV and thus is not seen by the recent nuclear res-

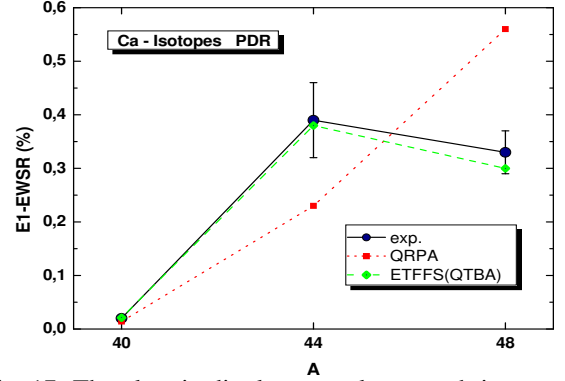Fig. 17: The electric dipole sum rule strength integrated up to 10 MeV is shown for the isotopes ^{40}Ca, ^{44}Ca, and ^{48}Ca. Black: experimental data; red: quasiparticle random phase approximation, green: extended theory of finite Fermi systems in the quasiparticle time blocking approximation.

onance fluorescence experiment. The calculation shows that the dipole states below 10 MeV are predominantly of isoscalar structure. This can be explained by the strongly attractive isoscalar force which brings down isoscalar strength from the giant resonance region. This finding is supported by $(\alpha, \alpha'\gamma)$ experiments.

3.7 Quantum interference in Au-Au collisions

Interference of probability amplitudes is at the basis of quantum mechanics. The most prominent example is the double slit experiment: one cannot know in principle through which slit the particle (*e.g.* an electron) went. It was shown recently how interference phenomena show up in so called ultraperipheral collisions (UPC). For example, two gold ions pass each other at the Relativistic Heavy Ion Collider RHIC at impact parameters larger than the sum of the nuclear radii. The electromagnetic field of one of the nuclei gives rise to an intense spectrum of photons, which extends up to very high energies. (The opportunities offered by UPC at relativistic heavy ion colliders were realized gradually during the past decades). A photon originating from one of the nuclei interacts with the other nucleus to coherently produce a vector meson in a diffractive interaction. Just as in the double slit experiment we do not know whether the nucleus coming from the right or the one from the left emitted the photon. We must take both possibilities into account when calculating the probability amplitude. We calculate the amplitudes for coherent vector meson production using semiclassical and Glauber (eikonal) methods. Especially we study inclusive cross sections as well as those where an additional mutual electromagnetic excitation of both ions takes place in addition to vector meson production. In order to describe vector meson production we use the vector dominance model and s-channel helicity conservation. The final state of the vector meson is characterized by its rapidity Y and the transverse momentum $v_\perp$.
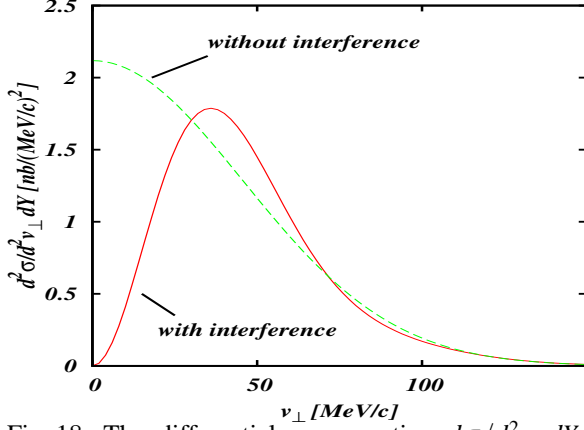
Fig. 18: The differential cross section $d\sigma/d^2v_\perp dY$ is shown as a function of the transverse momentum $v_\perp$ for J/Ψ production at mid-rapitity $Y = 0$ at LHC (Pb-Pb ions with γ=3000).

In Fig. 18 we show the differential cross section for $Y = 0$ as a function of the transverse momentum $v_\perp$ of the produced vector meson, with and without interference. The characteristic dip at small transverse momenta is the sign of the interference and it tells us about the details of the vector meson production amplitude. At RHIC ρ^0 production in UPC has been observed experimentally and first hints of this interference effect were presented at various conferences. One also expects to study this process at the LHC at CERN in the near future where in ultraperipheral collisions of Pb on Pb a 'lead flashlight' is produced. Due to the higher energies one also aims at observing the vector mesons J/Ψ and Υ. This process will allow to study the gluon distribution in nuclei. This will be part of a general program to study UPC at the LHC (Pb-Pb). So even when the nuclei do not interact strongly in violent central collisions we can learn very much about Quantum Chromodynamics in gentle ultraperipheral heavy ion collisions.

3.8 The sphere-plate Casimir effect

In 1948 the Dutch physicist H.B.G. Casimir predicted a very peculiar effect, the attraction between two metallic uncharged parallel plates in vacuum. The existence of such an interaction has been confirmed experimentally with *sufficient* accuracy only in the last decade. However, nearly all modern experiments study the attraction between a metallic sphere and a metallic plate which are much simpler to align than two plates, but much harder to calculate. In fact, with the exception of the proximity force *approximation* (PFA), which is applicable only for vanishing separation (note the splitting of the curves E and F in Fig. 19 for two equivalent, but different versions of the PFA), there does not exist a theoretical prediction for the Casimir energy of the sphere-plate system as function of the separation L. Therefore the corresponding Casimir effect for a fluctuating real scalar field between two spheres or one sphere and a plate came into the focus of theoretical research. An exact calculation of the

scalar Casimir energy for the case of two spheres is presented that contains the sphere-plate problem as a special case. The computation is based on a new Krein-type formula which directly expresses the geometry-dependent part of the density of states by the multi-scattering matrix of the pertinent scattering problem. The corresponding Casimir energy simply follows from the energy-integral over the multi-scattering phase shift (the logarithm of the multi-scattering determinant). The calculation is therefore not plagued by subtractions of the single-sphere contributions or by a removal of diverging ultra-violet contributions.
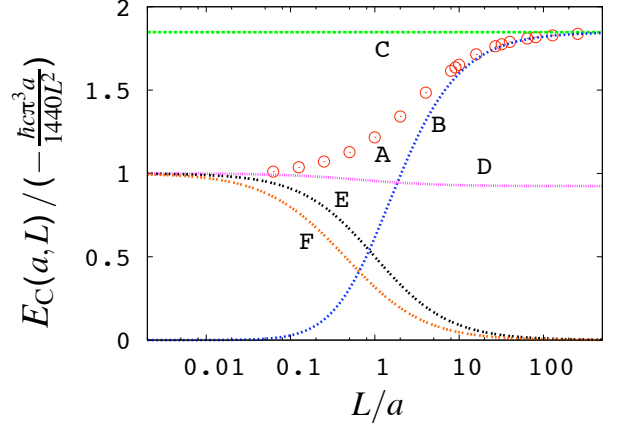

Fig. 19: Predictions for the scalar Casimir energy $\mathcal{E}_{\mathrm{C}}(a,L)$ of the Dirichlet sphere-plate configuration divided by the leading scale $-\hbar c\pi^3 a/1400L^2$ as function of the separation L between the surfaces in units of the radius a of the sphere. Circles (A) represent the exact data for the sphere-plate system, curve (B) shows the s-wave approximation, line (C) represents the predicted asymptotic limit $2 \times 90/\pi^4$, where $90/\pi^4$ is the asymptotic value of the semiclassical Gutzwiller formula including *all* repeats of the two-bounce periodic orbit (see line D). Curves (E) and (F) display the results of two different Ansätze for the proximity-force approximation.

The exact data for $L \geq 4a$ (see the circles A in Fig. 19), the s-wave approximation (curve B of Fig. 19), which works very nicely for $L \geq 15a$, and the corresponding asymptotic limit (line C of Fig. 19) are totally new results. Moreover, contrary to claims in the literature, the Casimir-Polder scaling of the scalar Casimir effect is excluded by the presented numerical *and* analytical results. The two-sphere and sphere-plane cases are only two examples, and the formalism presented can be easily extended to any number of spheres and planes as well (or disks and lines in two-dimensions). We have exemplified the calculation of the scalar Casimir energy only for the case of Dirichlet boundary conditions. One can replace the Dirichlet with Neumann boundary conditions or with any other conditions easily, or even replace the scatterers with arbitrary non-overlapping potentials/non-ideal reflectors.

4 COSY Operation and Developments

5 Preparations for FAIR

5.1 The PANDA experiment at the GSI

5.1.1 Introduction

One major component of the approved **F**acility for **A**ntiproton and **I**on **R**esearch (FAIR) at the GSI in Darmstadt is the **H**igh **E**nergy **S**torage **R**ing (HESR) with the PANDA (**P**roton **AN**tiproton **D**etector **A**rray) experiment. HESR will provide a phase space cooled antiproton beam of unsurpassed quality, precision and intensity. A momenta range up to 15 GeV/c will be covered allowing the detailed study both of the structure of hadrons in the charmonium mass range and the spectroscopy of double hyper nuclei. To serve this wide physics program the general purpose experiment PANDA is currently planned.

Basic concept of the detector is given by its division into two main parts, the central or target spectrometer and the forward spectrometer. This combines a nearly 4π coverage in the target region together with high acceptance of particles emitted at small polar angles in this fixed target kinematics.

The heart of the central spectrometer is a micro vertex detector located direct around the target for extreme precise tracking information. It is surrounded by the central tracker built either of straw tubes (STT) or a time projection chamber (TPC) in the barrel part, and a set of mini drift chambers (MDC) in the forward direction. Particle identification is done by two ring imaging Cherenkov counters surrounded by a compact electromagnetic calorimeter made out of $PbWO_4$ crystals. The entire system is situated in a 2 T solenoidal magnet which is covered outside with detectors for muon identification and tracking.

The forward spectrometer consists of a 2 T·m dipole magnet with a set of multiwire drift chambers (MuDC) for tracking, a RICH detector for particle identification, calorimeters for charged and neutral particles and a layer of muon counters.

The ongoing activities of the IKP for the PANDA detector are focused in three parts:

- the micro vertex detector
- the straw tube tracker
- the simulation of the tracking detectors

5.1.2 Micro vertex detector

The Micro Vertex Detector (MVD) plays a key role in the PANDA experiment to identify open charm and strangeness by detecting secondary decays of particles displaced from the primary interaction point. These decay lengths range from few 100 μm for charmed mesons and baryons up to several cm for strange hadrons. Main focus of the work of the last year was the optimization of the design concerning the demanding requirements, like high track density in forward direction, radiation background and low material budget. The result can be seen in Fig. 20. Altogether four sensitive layers are foreseen in the barrel part and six in the disk part covering the forward region. Due to the high occupancy and the radiation dose close to the interaction point the two innermost barrel layers and all inner parts of the disks have to be pixel detectors. For the outer layers strip detectors will be used taking advantage of their smaller material budget and fewer readout channels.
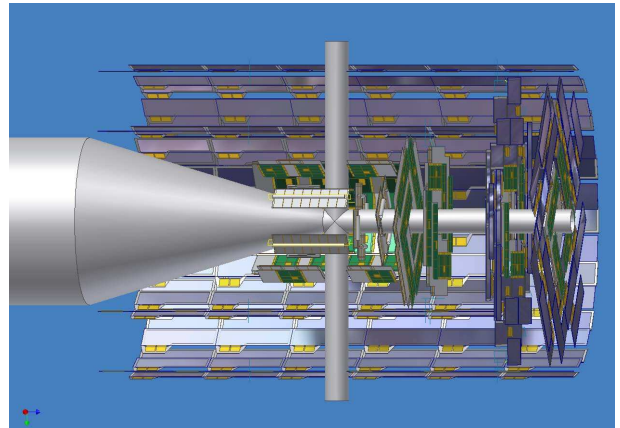

Fig. 20: Schematic view of the micro vertex detector, for visibility parts of some layers are omitted.

Extensive simulation studies have been carried out to evaluate the different design options and find the optimal layout combining high efficient track and vertex finding capabilities with smallest amount of material and readout channels. Some of these simulation results can be seen in Fig. 21 obtained for 10^7 $\bar{p}p$-annihilations per sec. at 15 GeV/c.

Figure 21 (a) shows for silicon the expected annual radiation damage in terms of 1 MeV n fluence. The most exposed detectors have to sustain a radiation level of several 10^{13} $n_{eq}cm^{-2}$ per year. Although this is roughly by a factor 5-6 less than the innermost LHC silicon detectors have to deal with it is still a fluence high enough requiring radiation tolerant technologies everywhere inside the MVD.

Figure 21 (b) refers to the material distribution inside the MVD volume taking all silicon components and part of the support structures into account. For all azimuth angles the radiation length of the total MVD is below 5% which limits the multi scattering of low momentum particles to reach the desired high precision tracking. In Fig. 21 (c) the number of hits per particle track is plotted showing an average of about 4–5 hits per track for nearly the entire acceptance volume. Only small holes in the acceptance due to the target pipe are visible.

Finally the simulated dE/dx for protons, kaons and pions in Fig. 21 (d) shows the possibility of using the charge information of the MVD for particle identification. For instance the MVD can contribute significantly to the pion-kaon separation below a momentum of 600 MeV/c if the silicon detectors measures the deposited charge with a reasonable resolution of about $1,000$ e$^-$.
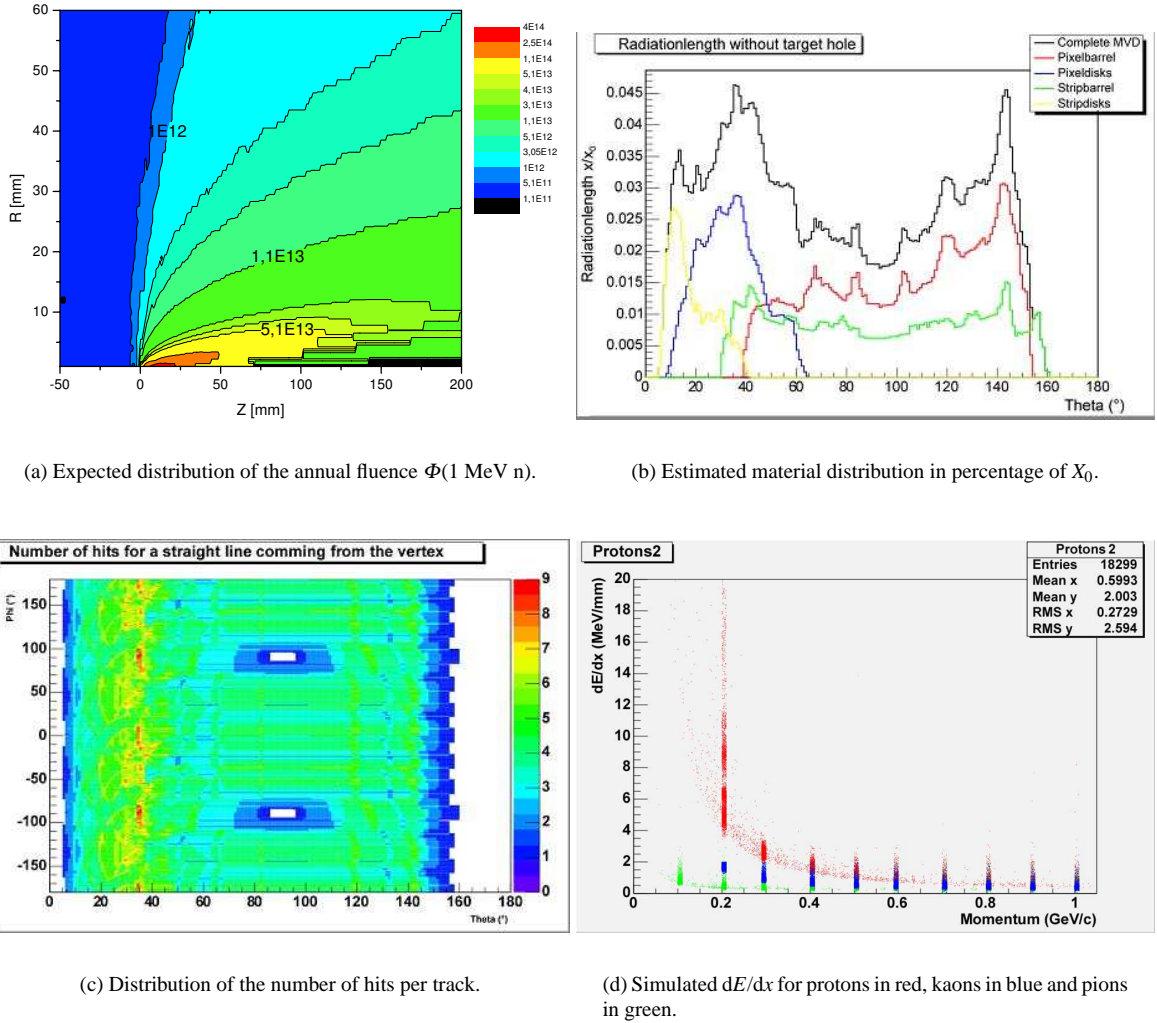
(a) Expected distribution of the annual fluence Φ(1 MeV n).

(b) Estimated material distribution in percentage of X_0.

(c) Distribution of the number of hits per track.

(d) Simulated dE/dx for protons in red, kaons in blue and pions in green.

Fig. 21: Selected simulation results for 10^7 $\bar{p}p$-annihilations per sec. at 15 GeV/c with the PANDA MVD .

Furthermore the detailed evaluation of existing technologies for the pixel part of the MVD is ongoing and especially the frond-end chips of the ATLAS and BTeV experiments are promising candidates for an usage in PANDA. Therefore in close collaboration with the ZEL a flexible, modular and free programmable readout system based on modern PCI and high speed optical data transmission technologies is currently under preparation.

5.1.3 Straw tube tracker

The main tracking element of the Panda target spectrometer is the Central Tracker (CT) which occupies a region inside the superconducting solenoid starting at a radial distance of 15 cm from the beam line, up to 42 cm. Along the beam (z) this region extends from 40 cm upstream to 110 cm downstream of the target. One of the proposed detector technologies currently under investigation for the CT is a straw tube tracker (STT). It consists of 11 double-layers of 150 cm long straw tubes which are

able to handle the high rate of 10^7 events per second with a multiplicity of 4–6 charged particles per event with a spatial resolution of 150 μm in both x and y directions.

Main focus of the current R&D for the STT done at IKP is the investigation of an alternative method to reconstruct the z-coordinate along the beam axis. Usually this information is gained by tilting the different layers by 2° to 3° towards each other. Another approach uses preamplifiers at both ends of the tube to calculate the z-coordinate of the track either by the amplitude ratio or the time difference between the two signals. Tremendous progress has been achieved during the last year showing the feasibility of both techniques although the measured resolutions do not yet match the PANDA requirements of several mm.

It turns out that for the time difference technique a simple discriminator followed by a TDC readout is sufficient to reach z-resolutions of 20–80 mm depending on the position along the straw axis, see Fig. 22 (a). For the charge amplitude technique a simple charge division approach leads to relatively poor results. But an improvement can
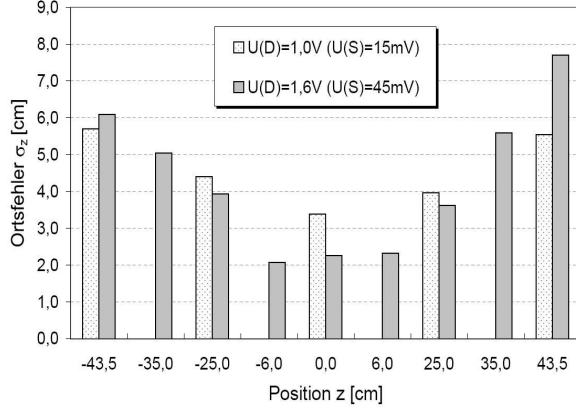
(a) Time difference technique, straw length 1.0 m.
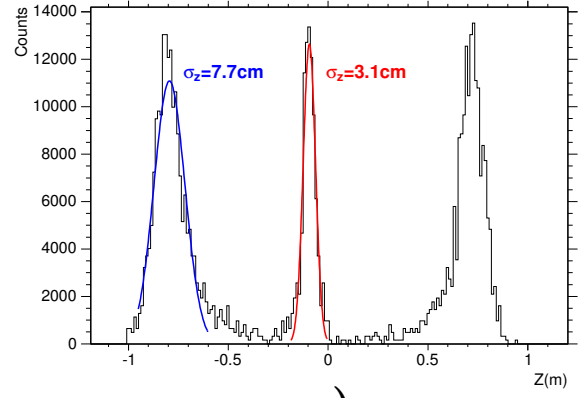
(b) Time dependent asymmetry technique, straw length 1.5 m.

Fig. 22: Resolutions along the straw axis illuminated with ^{90}Sr/^{90}Y using different z-position reconstruction techniques for a double sided readout; the two measurements in the left plot represent two settings of the preamplifiers.

be achieved by taking into the account the deformation of the signal shape due to timing effects caused by different signal propagation times ('time dependent asymmetry'). A reconstruction method was developed which uses this asymmetry to increase the accuracy for the z-measurement. As one can see in Fig. 22 (b) for a full size PANDA prototype straw a resolution of 30–70 mm has been reached. Although the results are encouraging the required z-resolution are failed by at least a factor of 3 so more effort is needed to improve further the accuracy of the z reconstruction.

5.1.4 Simulations

Of generally importance are Monte Carlo simulations of the detector which demonstrate if the proposed detector setup can fulfill the physics cases the detector is planed for. On the one hand comparisons between some detector configurations should give a rough indication for an ideal detector design as shown in Sect. 5.1.2, on the other hand several benchmark channels are selected which cover the most relevant physic topics. In particular also channels are chosen where PANDA can contribute significantly because of its unique properties. As an example the channel $\bar{p}p \rightarrow D^*_{sJ}(2317)^+ D^*_{sJ}(2317)^-$ is discussed here.

The narrow mesonic state $D^*_{sJ}(2317)^+$ originally discovered by BARBAR is identified as a scalar $c\bar{s}$-system with a significantly smaller mass and width than expected. BARBAR however, could only give an upper limit for this width which is smaller than 4.6 MeV whereas the theoretical predictions range from 10 to 200 keV. PANDA with the high quality HESR antiproton beam can solve this problem by measuring the excitation function of the reaction close to threshold. If the relative momentum spread of the incident beam is of the order 10^{-4} or better the cross section near threshold depends strongly on the en-

ergy and the width of the state, as one can see in Fig. 23.
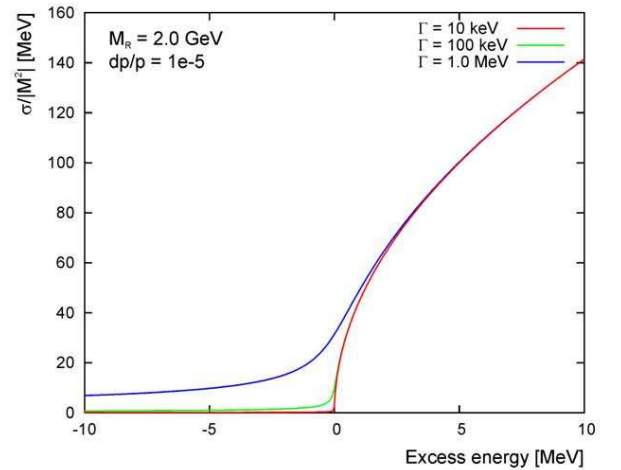
Fig. 23: Energy dependence of the simulated $D^*_{sJ}(2317)^+ D^*_{sJ}(2317)^-$ cross section for 10^{-5} relative momentum spread of the antiproton beam.

Therefore a width measurement with an precision of about 100 keV seems possible. Simulation studies using the PANDA simulation framework done at the IKP have shown that the $D^*_{sJ}(2317)^+$ mesonic state can be observed as a narrow resonance in the $D^*\pi^0$ invariant mass spectrum although the π^0 identification suffers from the huge combinatorial background due to electromagnetic split-offs.

A Councils

A.1 Scientific Council

Prof. J.P. Blaizot	CEA Saclay, FR	
Prof. P. Braun-Munzinger	GSI Darmstadt, DE	Chairperson
Prof. D.F. Geesaman	Argonne National Laboratory, U.S.A.	
Prof. H. Halling	ZEL, FZ-Jülich, DE	
Prof. M. Harakeh	KVI Groningen, NL (Chairman PAC)	
Prof. D. von Harrach	Universität Mainz, DE	
Prof. E. Hilger	Universität Bonn, DE	
Prof. Y. Nagai	RCNP Osaka, JP	
Prof. A.W. Thomas	Thomas Jefferson National Lab, U.S.A.	
Dr. D. Trines	DESY Hamburg, DE	

A.2 Program Advisory Committee

Prof. H. Freiesleben	TU Dresden, DE	
Prof. B. Friman	GSI Darmstadt, DE	
Prof. M. Garçon	CEA Saclay, FR	
Prof. M.N. Harakeh	KVI Groningen, NL	Chairperson
Prof. T. Johansson	Uppsala Universitet, SE	
Prof. R. Landua	CERN, CH	
Prof. V. Metag	Universität Gießen, DE	
Prof. W. Meyer	Universität Bochum, DE	
Prof. W.T.H. van Oers	University of Manitoba, CA	
Prof. E. Oset	Universitat de Valencia, ES	
Prof. E. Radermacher	CERN, CH	
Prof. C. Schaerf	INFN Roma II, IT	

B Personnel

Scientific Staff

Msc. M.-M. Abdel-Bary (E1)

Dr. Abdel Samad (E1)

DP S. An (GG)

Prof. Dr. G. Baur (TH) (a.o. Prof. Univ. Basel)

Dr. U. Bechstedt (GG)

DP A. Bogdanov (GG) until Jul., 2004

DP V. Bollini (E1) (until Feb. 5, 2004)

Dr. K. Bongardt (GG)

DI N. Bongers (GG)

DI W. Borgs (E2)

DI W. Bräutigam (GG)

DI R. Brings (GG)

DP A. Bubak (E1) (until Feb. 19, 2004)

Dr. M. Büscher (E2)

DP D. Chiladze (E2)

R. Czyzykiewicz (E1)

Dr. habil. J. Dietrich (GG) (PD Univ. Dortmund)

Dr. A. Djalois (E1)

DP A. Dzyuba (E2)

Dr. R Eichhorn (GG)

Dr. R. Engels (E2)

DI F.-J. Etzkorn (GG)

Dr. K. Fan (GG)

Dr. P. Fedorets (E2) (since Sep., 2004)

Dr. O. Felden (Rs)

Prof. Dr. D. Filges (E1) (apl. Prof. Univ. Wuppertal)
(until Jan 31, 2004)

DP M. Frink (TH) (until Oct. 31, 2004)

Dr. W. Gast (E1)

Dr. R. Gebel (GG)

Dr. habil. A. Gillitzer (E1) (PD Univ. Bonn)

Dr. habil. F.Goldenbaum (E1) (PD Univ. Wuppertal)

Dr. habil.D. Gotta (E2) (PD Univ. Köln)

Dr. F. Grümmer (TH)

Dr. D. Grzonka (E1)

Dr. habil. J. Haidenbauer (TH) (PD Univ. Graz)

Dr. C. Hanart (TH)

Dr. M. Hartmann (E2)

Dr. V. Hejny (E2)

DI K. Henn (GG)

DP V. Kamerdjiev (GG)

DP I. Keshelashvili (E2)

Prof Dr. K. Kilian (E1) (until Jul. 31, 2004)

DP D. Kirillov (GG) (since Oct. 19, 2004)

Dr. V. Kleber (E2)

Dr. St. Kliczewski (E1)

Prof. Dr. S. Krewald (TH) (apl. Prof. Univ. Bonn)

Th. Krings (Dt)

DI K. Kruck (GG)

Dr. P. Kulessa (E2)

Dr. A. Lehrach (GG)

DP V. Lenski (TH) (since Mar. 8, 2004)

DI B. Lensing (E1) (until Aug. 6, 2004)

DP V. Leontyev (E2)

DP M. Lesiak (E1) (since Sep. 1, 2004)

DP E. Lieder (E1) (until Oct. 31, 2004)

Dr. B. Lorentz (GG)

Prof. Dr. H. Machner (Prof. Univ. Duisburg-Essen)

Dr. Y. Maeda (E2)

Prof. Dr. R. Maier (GG) (Prof. Univ. Bonn)

DI J. Majewski (E2) (Jun. 1 to Dec. 31, 2004)

Dr. S. Martin (GG)

Prof. Dr. U.-G. Meißner (TH) (Prof. Univ. Bonn)

DI I. Mohos (GG)

Dr. H.-P. Morsch (E1)

Dr. P. Moskal (E1)

DP A. Mussgiller (E2)

Dr. M. Nekipelov (E2)

Prof. Dr. N. N. Nikolaev (TH)

Dr. K. Nünighoff (E1)

Prof. Dr. W. Oelert (E1) (apl. Prof. Univ Bochum)

Dr. H. Ohm (E2)

DI N. Paul (E1)

DP F. Pavlov (TH)

DP B. Piskor-Ignatowicz (E1) (since Mar., 1, 2004)

L. Platter (TH)

Dr. H. Polinder (TH) (since Jun., 14, 2004)

Dr. D. Prasuhn (GG)

DP D. Protic (Dt)

Dr. habil. F. Rathmann (E2) (PD Univ. Erlangen)

DI A. Richert (GG)

Prof. Dr. J. Ritman (E2) (Prof. Univ. Bochum)
(since Sep., 17, 2004)

Dr. E. Roderburg (E1)

Dr. P. v. Rossen (GG)

DP T. Rozek (E1)

DI J. Sarkadi (Ec)

DP F. Sassen (TH)

Dr. H. Schaal (E1)

Dr. S. Schadmand (E1) (since Sep. 1, 2004)

Dr. W. Schäfer (TH) (until Dec. 31, 2004)

Dr. R. Schleichert (E2)

Dr. A. Schnase (GG)

DP S. Schneider (TH) (until Apr. 30, 2004)

DI H. Schneider (GG)

DI G. Schug (GG)

Dr. Th. Sefzick (Ec)

DI E. Senicheva (GG) (since Apr. 1, 2004)

Dr. Y. Senichev (GG)

Dr. A. Sibirtsev (TH) (until Oct. 31, 2004)

DI M. Simon (GG)

DP A. Sokolov (E1) (since Aug. 1, 2004)

DI R. Stassen (GG)

Dr. H.-J. Stein (E2)

G. Sterzenbach (E1)

Dr. H. Stockhorst (GG)

Prof. Dr. H. Ströher (E2) (Prof. Univ. Köln)

Prof. Dr. J. Tang (GG) (until Mar. 12, 2004)

Dr. R. Tölle (GG)

DP A. Ucar (E1)

DP Y. Valdau (E2)

DI T. Vashegi (GG)

DP N. Vasiukhin (GG)

DP P. Vlasov (E1) (since Sep. 3, 2004)

Dr. K.-H. Watzlawik (E2)

J. Wimmer (E1)

DP P. Winter (E1)

Dr. P. Wintz (E1)

Dr. A. Wirzba (TH) (since Aug. 16, 2004;
      PD TU Darmstadt)

DI J.-D. Witt (GG)

Dr. M. Wolke (E2) (since July 1, 2004)

DP A. Wronska (E2) (until Aug. 30, 2004)

Dr. E. Zaplatin (GG)

DP D. Z. Zhang (E1) (since Oct. 10, 2004)

B.1 Technical and Administrative Staff

C. Berchem (Ec)

P. Birx (GG)

H.-G. Böge (GG) (until Nov. 30, 2004)

M. Böhnke (GG)

J. Borsch (GG)

P. Brittner (GG)

J. But (Ws)

M. Comuth (Ad)

W. Derissen (Cd)

N. Dolfus (Ec)

G. D'Orsaneo (E2)

R. Dosdall (E1) (since Sep., 2004)

B. Dahmen (GG)

C. Deliege (GG)

R. Enge (GG)

J. Engel (GG) (until Dec. 31, 2004)

B. Erkes (GG)

W. Ernst (Ec)

K. Esser (Ad)

H.-P. Faber (GG)

G. Fiori (Dt)

H.-W. Firmenich (Ws)

N. Gad (GG)

D. Gehsing (GG)

J. Göbbels (Rs)

H. Hadamek (Ws)

R, Hecker (GG)

E. Heßler (Cd)

M. Holona (Ws)

H.-M. Jäger (E1)

H. J. Jansen (Ws)

R. Jansen (Ad) (until Jul., 2004)

M. Karnadi (E2)

A. Kieven (GG)

K. Krafft (Rs)

Ch. Krahe (Ws)

M. Kremer (Ws)

G. Krol (GG)

M. Küven (Ws)

K.-G. Langenberg (GG)

G. Lürken (Ec)

H. Metz (Dt)

S. Müller (Ad)

R. Nellen (Ec)

H. Pütz (GG)

G. Roes (Ad)

N. Rotert (GG)

D. Ruhrig (GG)

T. Sagefka (GG)

F. Scheiba (GG)

H. Schiffer (Ec)

J. Schmitz (GG)

F. Schultheiß (Ws)

K. Schwill (Dt)

H. Singer (GG)

D. Spölgen (E2)

J. Strehl (Ws)

V.N. Tika (E1) (until Apr. 30, 2004)

J. Uehlemann (E1)

P. Wieder 9E2)

H. Zens (GG)

Ad = Administraion
Cd = Construction
Dt = Detectors
E1 = IKP-1
E2 = IKP-2
Ec = Electronics
GG = Accelerator Division
Rs = Radiation Safety
TH = Theory
Ws = Workshop

C Teaching Positions

Institute	Name	University
IKP-1	Dr. habil. A. Gillitzer	Bonn
	Dr. habil. F Goldenbaum	Wuppertal
	Prof. Dr. H. Machner	Essen
	Prof. Dr. W. Oelert	Bochum
	Prof. Dr. J. Ritman	Bochum
	Dr. habil. S. Schadmand	Giessen
IKP-2	Dr. habil. M. Büscher	Köln
	Dr. habil.D. Gotta	Köln
	Dr. habil. F. Rathmann	Erlangen-Nürnberg
	Prof. Dr. H. Ströher	Köln
Theory	Dr. habil. J. Haidenbauer	Graz
	Dr. habil. C. Hanhart	Bonn
	Prof. Dr. S. Krewald	Bonn
	Prof. Dr. U.-G. Meißner	Bonn
	Prof. Dr. N.N. Nikolaev	Moscow
	Dr. habil. A. Wirzba	Bonn
GG	Dr. habil. J. Dietrich	Dortmund
	Dr. A. Lehrach	Bonn
	Prof. Dr. R. Maier	Bonn

D Publications 2005

1. Experiment

1. **Determination of the $\bar{K}^0 d$ scattering length from the reaction $pp \to d\bar{K}^0 K^+$**
   A. Sibirtsev, M. Büscher, V.Yu. Grishina, C. Hanhart, L.A. Kondratyuk, S. Krewald, U.-G. Meißner
   *Phys. Lett. B **601** (2004) 132*

2. **$a_0^+(980)$ resonance production in the reaction $pp \to d\pi^+\eta$ close to the $K\bar{K}$ threshold**
   P. Fedorets, M. Büscher, V.P. Chernyshev, S. Dymov, V.Yu. Grishina, C. Hanhart, M. Hartmann, V. Hejny, V. Kleber, H.R. Koch, L.A. Kondratyuk, V. Koptev, A.E. Kudryavtsev, P. Kulessa, S. Merzliakov, S. Mikirtychiants, M. Nekipelov, H. Ohm, R. Schleichert, H. Ströher, V.E. Tarasov, K.-H. Watzlawik, I. Zychor
   subm. to Phys. Atom. Nucl. [Yad. Fiz.] [arXiv:nucl-ex/0501027]

3. **Near-threshold production of ω mesons in the $pn \to d\omega$ reaction**
   S. Barsov, I. Lehmann, R. Schleichert, C. Wilkin, M. Büscher, S. Dymov, Ye. Golubeva, M. Hartmann, V. Hejny, A. Kacharava, I. Keshelashvili, A. Khoukaz, V. Komarov, L. Kondratyuk, N. Lang, G. Macharashvili, T. Mersmann, S. Merzliakov, A. Mussgiller, M. Nioradze, A. Petrus, H. Ströher, Y. Uzikov, B. Zalikhanov
   *Eur. Phys. J. A **21** (2004) 507*

4. **Inclusive K^+-meson production in proton-nucleus interactions**
   M. Büscher, V. Koptev, M. Nekipelov, Z. Rudy, R. Schleichert, H. Ströher, Yu. Valdau, S. Barsov, M. Hartmann, V. Hejny, V. Kleber, N. Lang, I. Lehmann, N. Lang, S. Mikirtychiants, H. Ohm
   *Eur. Phys. J. A **22** (2004) 301*

5. **Measurement of the analyzing power in $\vec{p}d \to (pp)n$ with a fast forward $^1S_0$-diproton**
   S. Yaschenko, S. Dymov, V. Komarov, G. Macharashvili, F. Rathmann, S. Barsov, M. Hartmann, R. Gebel, A. Kacharava, A. Khoukaz, P. Kulessa, A. Kulikov, V. Kurbatov, N. Lang, I. Lehmann, B. Lorentz, T. Mersmann, S. Merzliakov, S. Mikirtytchiants, A. Mussgiller, M. Nioradze, H. Ohm, D. Prasuhn, R. Schleichert, H. Seyfarth, E. Steffens, H.J. Stein, H. Ströher, Yu. Uzikov, B. Zalikhanov, N. Zhuravlev
   *Phys. Rev. Lett. **94** (2005) 072304*

6. **Spectator detection for the measurement of proton-neutron interactions at ANKE**
   I. Lehmann, S. Barsov, R. Schleichert, C. Wilkin, M. Drochner, M. Hartmann, V. Hejny, S. Merzliakov, S. Mikirtychiants, A. Mussgiller, D. Protic, H. Ströher, S. Trusov, P. Wüstner
   *Nucl. Instr. Meth. A **530** (2004) 275*

7. **Experimental study of $pp\eta$ dynamics in the $pp \to pp\eta$ reaction**
   P. Moskal, H.H. Adam, A. Budzanowski, R. Czyżykiewicz, D. Grzonka, M. Janusz, L. Jarczyk, B. Kamys, A. Khoukaz, K. Kilian, P. Kowina, K. Nakayama, W. Oelert, C. Piskor-Ignatowicz, J. Przerwa, T. Rozek, R. Santo, G. Schepers, T. Sefzick, M. Siemaszko, J. Smyrski, S. Steltenkamp, A. Tächner, P. Winter, M. Wolke, P. Wüstner, W. Zipper
   *Phys. Rev. C **69** (2004) 025203*

8. **Total and differential cross sections for the $pp \to pp\eta'$ reaction near threshold**
   A. Khoukaz, I. Geck, C. Quentmeier, H.H. Adam, A. Budzanowski, R. Czyżykiewicz, D. Grzonka, L. Jarczyk, K. Kilian, P. Kowina, N. Lang, T. Lister, P. Moskal, W. Oelert, C. Piskor-Ignatowicz, T. Rozek, R. Santo, G. Schepers, T. Sefzick, S. Sewerin, M. Siemaszko, J. Smyrski, A. Strzałkowski, A. Täschner, P. Winter, M. Wolke, P. Wüstner, W. Zipper
   *Eur. Phys. J. A **20** (2004) 345*

9. **Energy dependence of the Λ/Σ° production cross section ratio in p-p interactions**
   P. Kowina, M. Wolke, H.H. Adam, A. Budzanowski, R. Czyżykiewicz, D. Grzonka, J. Haidenbauer, M. Janusz, L. Jarczyk, A. Khoukaz, K. Kilian, P. Moskal, W. Oelert, C. Quentmeier, C. Piskor-Ignatowicz, J. Przerwa, T. Rożek, R. Santo, G. Schepers, T. Sefzick, M. Siemaszko, J. Smyrski, S. Steltenkamp, A. Strzałkowski, P. Winter, P. Wüstner, W. Zipper
   *Eur. Phys. J. A **22** (2004) 293*

10. **Drift chamber with a c-shaped frame**
    J. Smyrski, Ch. Kolf, H.-H. Adam, A. Budzanowski, R. Czyzykiewicz, D. Grzonka, M. Janusz, L. Jarczyk, B. Kamys, A. Khoukaz, K. Kilian, W. Oelert, C. Piskor-Ignatowicz, J. Przerwa, T. Rozek, R. Santo, G. Schepers, T. Sefzick, M. Siemaszko, A. Taschner, P. Winter, M. Wolke, P. Wustner, W. Zipper
    Nucl. Instr. Meth. A, in print [arXiv:nucl-ex/0501023]

11. **A precision measurement of pp elastic scattering cross-sections at intermediate energies**
Albers,D., Bauer,F., Bisplinghoff,J., Bollmann,R., Büßer,K., Busch,M., Daniel,R., Diehl,O., Dohrmann,F., Engelhardt,H. P., Ernst,J., Eversheim,P. D., Gasthuber,M., Gebel,R., Greiff,J., Groß,A., Groß-Hardt,R., Heider,S., Heine,A., Hinterberger,F., Hüskes,T., Igelbrink,M., Jeske,M., Langkau,R., Lindlein,J., Maier,R., Maschuw,R., Mosel,F., Prasuhn,D., Rohdjeß,H., Rosendaal,D., von Rossen,P., Scheid,N., Schirm,N., Schulz- Rojahn,M., Schwandt,F., Schwarz,V., Scobel,W., Thomas,S., Trelle,H.-J., Weise,E., Welinghausen,A., Woller,K., Ziegler,R.
Eur. Phys. J. A **22** *(2004) 125*

12. **Evidence for a narrow resonance at 1530 MeV/c^2 in the $K°p$ system of the reaction $pp \to \Sigma^+ K° p$ from the COSY-TOF experiment**
M. Abdel-Bary, S. Abdel-Samad, K.Th. Brinkmann, H. Clement, E. Doroshkevich, M. Drochner, S. Dshemuchadse, A. Erhardt, W. Eyrich, D. Filges, A. Filippi, H. Freiesleben, M. Fritsch, J. Georgi, A. Gillitzer, D. Hesselbarth, R. Jakel, B. Jakob, L. Karsch, K. Kilian, H. Koch, J. Kress, E. Kuhlmann, S. Marcello, S. Marwinski, R. Meier, P. Michel, K. Moller, H. Mortel, H.P. Morsch, N. Paul, L. Pinna, C. Pizzolotto, M. Richter, E. Roderburg, P. Schonmeier, W. Schroeder, M. Schulte-Wissermann, T. Sefzick, F. Stinzing, G.Y. Sun, A. Teufel, A. Ucar, G.J. Wagner, M. Wagner, A. Wilms, P. Wintz, St. Wirth, P. Wüstner
Phys. Lett. B **595** *(2004) 127*

13. **Detailed comparison of the $pp \to \pi^+ pn$ and $pp \to \pi^+ d$ reactions at 951 MeV**
M. Abdel-Bary, A. Budzanowski A. Chatterjee, J. Ernst, P. Hawranek, F. Hinterberger, V. Jha, K. Kilian, S. Kliczewski, D. Kirillov, D. Kolev, M. Kravcikova, T. Kutsarova, M. Lesiak, J. Lieb, H. Machner, A. Magiera, R. Maier, G. Martinska, S. Nedev, J. Niskanen, N. Piskunov, D. Prasuhn, D. Protic, P. von Rossen, B.J. Roy, I. Sitnik, R. Siudak, M. Smiechowicz, R. Tsenov, M. Ulicny, J. Urban, G. Vankova, C. Wilkin
Phys. Lett. B **610** *(2005) 31*

14. **A precision experiment determining the η meson mass**
M. Abdel-Bary, A. Budzanowski A. Chatterjee, J. Ernst, P. Hawranek, R. Jahn, V. Jha, K. Kilian, S. Kliczewski, D. Kirillov, D. Kolev, M. Kravcikova, T. Kutsarova, M. Lesiak, J. Lieb, H. Machner, A. Magiera, R. Maier, G. Martinska, S. Nedev, N. Piskunov, D. Prasuhn, D. Protic, P. von Rossen, B.J. Roy, I. Sitnik, R. Siudak, M. Smiechowicz, H. J. Stein, R. Tsenov, M. Ulicny, J. Urban, G. Vankova, C. Wilkin
subm. to Phys. Lett. B

15. **PISA — an experiment for fragment spectroscopy at the internal beam of COSY: application of an axial ionization chamber**
R. Barna, V. Bollini, A. Bubak, A. Budzanowski, D. De Pasquale, D. Filges, S. Förtsch, F. Goldenbaum, A. Heczko, H. Hodde, A. Italiano, L. Jarczyk, B. Kamys, J. Kisiel, M. Kistryn, St. Kistryn, St. Kliczewski, P. Kulessa, H. Machner, A. Magiera, J. Majewski, W. Migdał, H. Ohm, N. Paul, B. Piskor-Ignatowicz, K. Pysz, Z. Rudy, H. Schaal, R. Siudak, E. Stephan, D. Steyn, R. Sworst, T. Thovhogi, M. Wojciechowski, W. Zipper
Nucl. Instrum. Meth. A **519** *(2004) 610*

16. **Parameterization of the total cross-section for (p,^{7}Be) reaction**
A.Bubak, B. Kamys, M.Kistryn, B.Piskor-Ignatowicz
Nucl. Instrum. Meth. B **226** *(2004) 507*

17. **Ice moderator experiments at very low temperatures**
K. Nuenighoff, Ch. Pohl, V. Bollini, A. Bubak, H. Conrad, D. Filges, H. Glueckler, F. Goldenbaum, G. Hansen, B. Lensing, R.-D. Neef, N. Paul, D. Prasuhn, K. Pysz, H. Schaal, H. Soltner, H. Stelzer, H. Tietze-Jaensch, W. Bernnat, J. Keinert, M. Mattes, W. Ninaus, S. Koulikov, A. Smirnov, M. Wohlmuther
Eur. Phys. J. A **22** *(2004) 519*

18. **First laser-controlled antihydrogen production**
C.H. Storry, A. Speck, D. Le Sage, N. Guise, G. Gabrielse, D. Grzonka, W. Oelert, G. Schepers, T. Sefzick, H. Pittner, M. Herrmann, J. Walz, T.W. Hänsch, D. Comeau, and E. A. Hessels
Phys. Rev. Lett. **93** *(2004) 263401*

19. **Observations of cold antihydrogen**
J.N. Tan, N.S. Bowden, G. Gabrielse, P. Oxley, A. Speck, C.H. Storry, M. Wessels, D. Grzonka, W. Oelert, G. Schepers, T. Sefzick, J. Walz, H. Pittner, T.W. Hänsch, E.A. Hessels
Nucl. Instr. Meth. B **214** *(2004) 22*

20. **Aperture method to determine the density and geometry of anti-particle plasmas,**
P. Oxley, N. S.Bowden, R. Parrott, A. Speck, C. Storry, J.N. Tan, M. Wessels, G. Gabrielse, D. Grzonka, W. Oelert,

G. Schepers, T. Sefzick, J. Walz, H. Pittner, T.W. Hänsch, and E. A. Hessels
Phys. Lett. B **595** *(2004) 60*

21. **First measurement of the velocity of slow antihydrogen atoms,**
G. Gabrielse, A. Speck and C.H. Storry, D. Le Sage, N. Guise, D. Grzonka, W. Oelert, G. Schepers, T. Sefzick, H. Pittner, J. Walz, T.W. Hänsch, D. Comeau, E.A. Hessels
Phys. Rev. Lett. **93** *(2004) 073401*

22. **Precision spectroscopy of light exotic atoms**
D. Gotta
Prog. Part. and Nucl. Phys. **52** *(2004) 133*

23. **On the characterization of a Bragg spectrometer with X-rays from an ECR source**
D.F. Anagnostopoulos, S. Biri, D. Gotta, A. Gruber, P. Indelicato, B. Leoni, H. Fuhrmann, L.M. Simons, L. Stingelin, A. Wasser, J. Zmeskal
Nucl. Instr. Meth. A, to be published

24. **Studies of multi-nucleon transfer reactions in ^{90}Zr(^{18}O,X) and ^{90}Zr(^{16}O,X)**
V. Jha, B. J. Roy, A. Chatterjee, H. Machner
Eur. Phys. J. A **19** *(2004) 347*

25. **Exclusive η production in proton induced reactions**
F.Balestra, Y.Bedfer, R.Bertini, L.C.Bland, A.Brenschede, F.Brochard, M.P.Bussa, Seonho Choi, M.L. Colantoni, R. Dressler, M. Dzemidzic, J.-Cl. Faivre, A. Ferrero, L. Ferrero, J. Foryciarz, I. Frohlich, V. Frolov, R. Garfagnini, A. Grasso, S. Heinz, W.W. Jacobs, W. Kuhn, A. Maggiora, M. Maggiora, A. Manara, D. Panzieri, H.-W. Pfaff, G. Piragino, A. Popov, J. Ritman, P. Salabura, V. Tchalyshev, F. Tosello, S.E. Vigdor, G. Zosi (DISTO collaboration)
Phys. Rev. C. **69** *(2004) 064003*

26. **Production of ϕ mesons in Au+Au collisions at 11.7 A GeV/c**
B.B. Back, R.R. Betts, J. Chang, W.C. Chang, C.Y. Chi, Y.Y. Chu, J.B. Cumming, J.C. Dunlop, W. Eldredge, S.Y. Fung, R. Ganz, E. Garcia, A. Gillitzer, G. Heintzelman, W.F. Henning, D.J. Hofman, B. Holzman, J.H. Kang, E.J. Kim, S.Y. Kim, Y. Kwon, D. McLeod, A.C. Mignerey, M. Moulson, V. Nanal, C.A. Ogilvie, R. Pak, A. Ruangma, D.E. Russ, R.K. Seto, P.J. Stanskas, G.S.F. Stephans, H.Q. Wang, F.L.H. Wolfs, A.H. Wuosmaa, H. Xiang, G.H. Xu, H.B. Yao, C.M. Zou (BNL-E917 Collaboration)
Phys. Rev. C **69** *(2004) 054901*

27. **Precision spectroscopy of pionic 1s states of Sn nuclei and evidence for partial restoration of chiral symmetry in the nuclear medium**
K. Suzuki, M. Fujita, H. Geissel, H. Gilg, A. Gillitzer, R.S. Hayano, S. Hirenzaki, K. Itahashi, M. Iwasaki, P. Kienle, M. Matos, G. Münzenberg, T. Ohtsubo, M. Sato, M. Shindo, T. Suzuki, H. Weick, M. Winkler, T. Yamazaki, and T. Yoneyama
Phys. Rev. Lett. **92** *(2004) 072302*

28. **Axial observables in $\vec{d}\vec{p}$ breakup and the three-nucleon force**
H.O. Meyer, T.J. Whitaker, R.E. Pollock, B.v. Przewoski, T. Rinckel, J. Doskow, J. Kuros-Zolnierczuk, P. Thörngren-Engblom, P.V. Pancella, T. Wise, B. Lorentz, F. Rathmann
Phys. Rev. Lett. **93** *(2004) 112502*

29. **Analyzing powers and spin correlation coefficients for p+d elastic scattering at 135 and 200 MeV**
B.v. Przewoski, H.O. Meyer, J.T. Balewski, W.W. Daehnick, J. Doskow, W. Haeberli, R. Ibald, B. Lorentz, R.E. Pollock, P.V. Pancella, F. Rathmann, T. Rinckel, Swapan K. Saha, B. Schwartz, P. Thörngren-Engblom, A. Wellinghausen, T.J. Whitaker, T. Wise, H. Witala
Phys. Rev. C, accepted for publication

30. **Conceptual design and simulation of the PANDA detector**
J. Ritman
Nucl. Instrum. Meth. B **214** *(2004) 201*

31. **A method to polarize stored antiprotons to a high degree**
F. Rathmann, P. Lenisa, E. Steffens, M. Contalbrigo, P.F. Dalpiaz, A. Kacharava, A. Lehrach, B. Lorentz, R. Maier, D. Prasuhn, H. Ströher,
Phys. Rev. Lett. **94** *(2005) 014801*

2. Theory

32. **Accessing transversity via J/Ψ production in polarized $p\bar{p}$ interactions**
Anselmino, M.; Barone, V.; Drago, A.; Nikolaev, N. N.
Phys. Lett. B **594** *(2004) 97*

33. **Evidence that the $a_0(980)$ and $f_0(980)$ are not elementary particles**
Baru, V.; Haidenbauer, J.; Hanhart, C.; Kalashnikov, Yu.; Kudryavtsev, A.
Phys. Lett. B **586** *(2004) 53*

34. **The role of the nucleon recoil in low-energy meson nucleus reactions**
Baru, V.; Hanhart, C.; Kudryavtsev, A. E.; Meißner, U.-G.
Phys. Lett. B **589** *(2004) 118*

35. **Flatte-like distributions and the $a_0(980)/f_0(980)$ mesons**
Baru, V.; Haidenbauer, J.; Hanhart, C.; Kudryavtsev, A.; Meißner, U.-G.
Eur. Phys. J. A **23***, (2005) 523*

36. **Theory of the Trojan-horse method**
Baur, G.; Typel, S.
Prog. Theor. Phys. Suppl. **154** *(2004) 333*

37. **Radiative neutron beta-decay in effective field theory**
Bernard, V.; Gardner, S.; Meißner, U.-G.; Zhang, C.
Phys. Lett. B **593** *(2004) 105*

38. **Cutoff schemes in chiral perturbation theory and the quark mass expansion of the nucleon mass**
Bernard, V.; Hemmert, T. R.; Meißner, U.-G.
Nucl. Phys. A **732** *(2004) 149*

39. **Infrared regularization for spin-1 fields**
Bruns, P. C.; Meißner, U.-G.
Eur. Phys. J. C, in print [arXiv:hep-ph/0411223]

40. **Improving the convergence of the chiral expansion for nuclear forces I: Peripheral phases**
Epelbaum, E.; Glöckle, W.; Meißner, U.-G.
Eur. Phys. J. A **19** *(2004) 125*

41. **Improving the convergence of the chiral expansion for nuclear forces II: Low phases and the deuteron**
Epelbaum, E.; Glöckle, W.; Meißner, U.-G.
Eur. Phys. J. A **19** *(2004) 401*

42. **The two-nucleon system at next-to-next-to-next-to-leading order**
Epelbaum, E.; Glöckle, W.; Meißner, U.-G.
Nucl. Phys. **A 747** *(2005) 362*

43. **Isospin dependence of the three-nucleon force**
Epelbaum, E.; Meißner, U.-G.; Palomar, J. E.
Phys. Rev. C **71** *(2005) 024001*

44. **Chiral extrapolations of baryon masses for unquenched three-flavor lattice simulations**
Frink, M.; Meißner, U.-G.
JHEP **07** *(2004) 028*

45. **Survey of charge symmetry breaking operators for $dd \to \alpha\pi^0$**
Gardestig, A.; Horowitz, C. J.; Nogga, A.; Fonseca, A. C.; Hanhart, C.; Miller, G. A.; Niskanen, J. A.; van Kolck, U.
Phys. Rev. C **69** *(2004) 044606*

46. **Radiative tritium β-decay and the neutrino mass**
Gardner, S.; Bernard, V.; Meißner, U.-G.
Phys. Lett. B **598** *(2004) 188*

47. **How to extract the ΛN scattering length from production reactions**
Gasparyan, A.; Haidenbauer, J.; Hanhart, C.; Speth, J.
Phys. Rev. C **69** *(2004) 034006*

48. **Near threshold production of $a_0(980)$-mesons in the reaction $pp \to dK^+\bar{K}^0$**
V.Yu. Grishina, L.A. Kondratyuk, M. Büscher, W. Cassing
Eur. Phys. J. A **21** *(2004) 507*

49. **On the pion cloud of the nucleon**
Hammer, H.-W.; Drechsel, D.; Meißner, U.-G.
Phys. Lett. B **586** *(2004) 291*

50. **Updated dispersion-theoretical analysis of the nucleon electromagnetic form factor**
Hammer, H.-W.; Meißner, U.-G.
Eur. Phys. J. A **20** *(2004) 469*

51. **How to measure the parity of the Θ^+ in $\vec{p}\vec{p}$ collisions**
C. Hanhart, M. Büscher, W. Eyrich, K. Kilian, U.-G. Meißner, F. Rathmann, A. Sibirtsev, and H. Ströher
Phys. Lett. B **590** *(2004) 39*

52. **Meson production in nucleon-nucleon collisions close to the threshold**
Hanhart, C.
Phys. Rep. **397** *(2004) 155*

53. **On the determination of the parity of the Θ^+**
Hanhart, C.; Haidenbauer, J.; Nakayama, K.; Meissner, U.-G.
Phys. Lett. B **606** *(2005) 67*

54. **Comment on "Photoproduction of η mesic ^{3}He"**
Hanhart, C.
Phys. Rev. Lett. **94** *(2005) 049101*

55. **A cluster version of the GGT sum rule**
Hencken, K.; Baur, G.; Trautmann, D.
Nucl. Phys. A **733** *(2004) 200*

56. **Production of QED pairs at small impact parameter in relativistic heavy ion collisions**
Hencken, K.; Trautmann, D.; Baur, G.
Phys. Rev. C **69** *(2004) 054902*

57. **Parity nonconserving observables in thermal neutron capture on a proton**
Hyun, C.H.; Lee, S.J.; Haidenbauer, J.; Hong, S.W.
Eur. Phys. J. A, in print [arXiv:nucl-th/0411102]

58. **Improved analysis of coherent neutral pion electroproduction on deuterium in chiral perturbation theory**
Krebs, H.; Bernard, V.; Meißner, U.-G.
Eur. Phys. J. A **22** *(2004) 503*

59. **Orthonormalization procedure for chiral effective nuclear field theory**
Krebs, H.; Bernard, V.; Meißner, U.-G.
Ann. Phys. **316** *(2005) 160*

60. **Lifetime of kaonium**
Krewald, S.; Lemmer, R. H.; Sassen, F. P.
Phys. Rev. D **69** *(2004) 016003*

61. **Spectrum and decays of kaonic hydrogen**
Meißner, U.-G.; Raha, U.; Rusetsky, A.
Eur. Phys. J. C **35** *(2004) 349*

62. **Evolution of high-mass diffraction from the light quark valence component of the Pomeron**
Nikolaev, N. N.; Schäfer, W.; Zakharov, B. G.; Zoller, V. R.
JETP Lett. **80** *(2004) 6, 371*

63. **Four-boson system with short-range interactions**
    Platter, L.; Hammer, H.-W.; Meißner, U.-G.
    Phys. Rev. A **70** *(2004) 052101*

64. **Universal properties of the four-boson system in two dimensions**
    Platter, L.; Hammer, H.-W.; Meißner, U.-G.
    Few-Body Systems **35** *(2004) 169*

65. **On the correlation between the binding energies of the triton and the alpha-particle**
    Platter, L.; Hammer, H.-W.; Meißner, U.-G.
    Phys. Lett. **B 607** *(2005) 254*

66. **The η-^{3}He scattering length revisited**
    Sibirtsev, A.; Haidenbauer, J.; Hanhart, C.; Niskanen, J.
    Eur. Phys. J. A **22** *(2004) 495*

67. **New results on the limit for the width of the exotic Θ^+ resonance**
    Sibirtsev, A.; Haidenbauer, J.; Krewald, S.; Meißner, U.-G.
    Phys. Lett. B **599** *(2004) 230*

68. **Bounds on the bound η-^{3}He system**
    Sibirtsev, A.; Haidenbauer, J.; Niskanen, J.; Meißner, U.-G.
    Phys. Rev. C **70** *(2004) 047001*

69. **Systematic analysis of charmonium photoproduction**
    Sibirtsev, A.; Krewald, S.; Thomas, A. W.
    Jour. Phys. G **30** *(2004) 1427*

70. **Analysis of Θ^+ production in K^+Xe collisions**
    Sibirtsev, A.; Haidenbauer, J.; Krewald, S.; Meißner, U.-G.
    Eur. Phys. J. A **23** *(2005) 491*

71. **Near threshold enhancement of the $p\bar{p}$ mass spectrum in J/Ψ decay**
    Sibirtsev, A.; Haidenbauer, J.; Krewald, S.; Meißner; U.-G., Thomas, A.W.;
    Phys. Rev. D, in print [arXiv:hep-ph/0411386]

72. **Extended theory of finite Fermi systems: collective vibrations in closed shell nuclei**
    Speth, J.; Kamerdzhiev, S.; Speth, J.; Tertychny, G.
    Phys. Rep. **393** *(2004) 1*

73. **Effective-range approach and scaling laws for electromagnetic strength in neutron-halo nuclei**
    Typel, S.; Baur, G.
    Phys. Rev. Lett. **93** *(2004) 142502*

74. **Nucleon-nucleon potential in finite nuclei**
    Yakhshiev, U. T.; Meißner, U.-G.; Wirzba, A.; Rakhimov,A. M.; Musakhanov, M. M.
    Phys. Rev. C, **71** *(2005) 034007*

3. Accelerator

75. **Achieving 99.9% proton spin-flip efficiency at higher energy with a small rf-dipole**
    Leonova,M. A., Krisch,A. D., Morozov,V. S., Raymond,R. S., Wong,V. K., Gebel,R., Lehrach,A., Lorentz,B., Maier,R., Prasuhn,D., Schnase,A., Stockhorst,H., Eversheim,D. P., Hinterberger,F., Ulbrich,K.
    Phys. Rev. Lett. **93** *(2004) 224801*

76. **Ion sources and low energy beam transport for the new superconducting injector linac for COSY/Jülich**
    Gebel,R., Felden,O., von Rossen,P.
    Rev. of Sci. Instr. **75** *(2004) 5, 1860*

77. **Instability phenomena of electron-cooled ion beams at COSY**
    Kamerdzhiev,V., Dietrich,J., Maier,R., Meshkov,I., Mohos,I., Prasuhn,D., Sidorin,A., Stein,H. J., Stockhorst,H.
    Nucl. Instr. and Meth. A **532** *(2004) 1/2, 285*

78. **Stripping injection at synchrotrons with electron cooling**
Meshkov,I. N., Sidorin,A. O., Stein,J., Dietrich,J., Kamerdzhiev,V.
Phys. of Part. and Nucl. **120** *(2004) 3, 4*

79. **Spin manipulation of 1.94 gev/c polarized protons stored in the COSY Cooler Synchrotron**
Morozov,V. S., Krisch,A. D., Leonova,M. A., Raymond,R. S., Wong,V. K., Yonehara,K., Bechstedt,U., Gebel,R., Lehrach,A., Lorentz,B., Maier,R., Prasuhn,D., Schnase,A., Stockhorst,H., Eversheim,D. P., Hinterberger,F., Rohdjeß,H., Ulbrich,K.
Phys. Rev., Accelerators and Beams **7** *(2004) 024002*

80. **Spin-flipping polarized deuterons at COSY**
Yonehara,J. C., Krisch,A. D., Morozov,V., Raymond,R. S., Wong,V. K., Bechstedt,U., Gebel,R., Lehrach,A., Lorentz,B., Maier,R., Prasuhn,D., Schnase,A., Stockhorst,H., Eversheim,D. P., Hinterberger,F., Rohdjess,H., Ulbrich,K., Scobel,W.
Inters. of Part. and Nucl. Phys. 8th Conf. 0-7354-0169-1. - 763 - 766

81. **Separatrix formalism applied to linacs accelerating particles with different charge to mass ratio**
Bogdanov,A., Maier,R., Senichev,Y
Proc. EPAC, Lucerne, CH, (2004) 92-9083-231-2. - 1252 - 1254

82. **Delta-T procedure for superconducting linear accelerator**
Bogdanov,A., Maier,R., Senichev,Y.
Proc. EPAC, Lucerne, CH, (2004) 92-9083-231-2. - 1249

83. **Beam position monitor development for the iThemba LABS cyclotron beamlines**
Dietrich,J., Mohos,I., Botha,A. H., Conradie,J. L., Delsink,J. L. G., Rohwer,P. F
Proc. EPAC, Lucerne, CH, (2004) 92-9083-231-2. - 2589 - 2591

84. **Luminosity considerations for internal and external experiments at COSY**
Lehrach,A., Bechstedt,U., Dietrich,J., Eichhorn,R., Gebel,R., Lorentz,B., Maier,R., Prasuhn,D., Schneider,H., Stassen,R., Stockhorst,H., Tölle,R.
Proc. EPAC, Lucerne, CH, (2004) 92-9083-231-2. - 1255 - 1257

85. **Status of the Cooler Synchrotron COSY-Jülich**
Lorentz,B., Bechstedt,U., Dietrich,J., Eichhorn,R., Gebel,R., Lehrach,A., Maier,R., Prasuhn,D., Schnase,A., Schneider,H., Stassen,R., Stockhorst,H., Tölle,R.
Proc. EPAC, Lucerne, CH, (2004) 92-9083-231-2. - 1246 - 1248

86. **High field gradient cavity for J-PARC 3 GeV RCS**
Ohmori,C., Anami,S., Ezura,E., Hara,K., Hashimoto,Y., Takagi,A., Toda,M., Yoshii,M., Nomura,M., Schnase,A., Tamura,F., Yamamoto,M.
Proc. EPAC, Lucerne, CH, (2004) 92-9083-231-2. - 123 - 125

87. **Methods and instrumentation for measurement of low ion beam currents at the cryring**
Paal,A., Källberg,A., Simonsson,A., Dietrich,J., Mohos,I.
Proc. EPAC, Lucerne, CH, (2004) 92-9083-231-2. - 2748 - 2749

88. **Lattice design study for HESR**
Senichev,Y., An,S., Bongardt,K., Eichhorn,R., Lehrach,A., Maier,R., Martin,S., Prasuhn,D., Stockhorst,H., Tölle,R.
Proc. EPAC, Lucerne, CH, (2004) 92-9083-231-2. - 653 - 655

89. **First results of pulsed superconducting half-wave resonators**
Stassen,R., Eichhorn,R., Esser,F. M., Laatsch,B., Maier,R., Schug,G., Tölle,R.
Proc. EPAC, Lucerne, CH, (2004) 92-9083-231-2. - 1258 - 1260

90. **Space charge problem in low energy super-conducting accelerators**
Vasyukhin,N. E., Maier,R., Senichev,Y.
Proc. EPAC, Lucerne, CH, (2004) 92-9083-231-2. - 1999 - 2001

91. **Dual harmonic acceleration with broadband ma Cavities in J-PARC RCS**
Yamamoto,M., Anami,S., Ezura,E., Hara,K., Hashimoto,Y., Ohmori,C., Takagi,A., Yoshii,M., Nomura,M., Schnase,A., Tamura,F.
Proc. EPAC, Lucerne, CH, (2004) 92-9083-231-2. - 1318 - 1320

92. **Triple-spoke cavities in FZJ**
Zaplatin,E., Braeutigam,W., Maier,R., Pap,M., Skrobucha,M., Stassen,R., Tölle,R.
Proc. EPAC, Lucerne, CH, (2004) 92-9083-231-2. - 1261 - 1263

4. Others

93. **Detection characteristics of Ge detectorsl with microstructured amorphous Ge contacts**
Protic,D., Krings,T.
IEEE Trans. on Nuc. Sci., 51 (2004), 1129 - 1133

94. **Time scales involved in emergent market coherence**
Kwapien, J.; Drozdz, S.; Speth, J.
*Physica A **337** (2004) 231 - 242*

95. **Zur Dämpfung der Globalisierung**
Otto W.B. Schult
*Die Neue Ordnung **58** (2004) 264 - 279*

E Beam Time at COSY 2005

Date	Experiment	Duration	Reaction
14.01.05–24.01.05	ANKE	1 week	$dp \to {}^3\mathrm{He}\eta$
28.01.–09.02.	GEM	2 weeks	$\vec{d}d \to {}^4\mathrm{He}\eta$
11.02.–21.02.	ANKE	1 week	$\vec{d}p \to (pp)n$
21.02.–24.02.	ANKE	1 week	cell tests
25.02.–14.03.	ANKE	2 weeks	$dd \to {}^3AN\pi$
14.03.–04.04.	ANKE	3 weeks	$pp \to ppK^+K^-$
08.04.–02.05.	COSY-11	3 weeks	$dp \to {}^3\mathrm{H}\pi^+/{}^3\mathrm{He}\pi^0$
06.05.–23.05.	GEM	2 weeks	$pA \to X$
27.05.–13.06.	PISA	2 weeks	$pA \to$ spallation
09.09.–26.09.	HIRES	2 weeks	$pp \to pK^+\Lambda$
30.09.–10.10.	COSY-11	1 week	$pp \to ppK^+K^-$
21.10.–07.11.	COSY-11	2 weeks	$\vec{p}p \to pK^+\Lambda$
11.11.–21.11.	SPIN@COSY	1 week	spin manipulation
21.11.–05.12.	ANKE	2 weeks	cell tests
Total '05		25 weeks	

F Contents of the Attached CD